International Journal of Mechanical Sciences 278 (2024) 109441

Contents lists available at ScienceDirect

International Journal of Mechanical Sciences

journal homepage: www.elsevier.com/locate/ijmecsci

Effect of compressibility on the mechanics of hyperelastic membranes

Stefano Sirotti, Matteo Pelliciari *, Angelo Marcello Tarantino

DIEF, Department of Engineering "Enzo Ferrari", via P. Vivarelli 10, 41125 Modena, Italy

ARTICLE INFO

Keywords:
Inflated membranes
Volumetric deformations
Nonlinear solutions
Finite elasticity

ABSTRACT

Elastic membranes are usually studied assuming material incompressibility. However, in several applications they are made of compressible materials such as polymeric foams, hydrogels, and certain kinds of elastomers. Only a few works attempted to incorporate volume changes into membrane problems, but with significant limitations. The models proposed were designed for nearly incompressible materials and lacked a foundation in experimental data, leading to results of limited value. In this work, we investigate the effect of compressibility in membrane problems adopting a consistent model based on the real response of materials to large volume changes. We consider three benchmark problems of nonlinear elasticity: (i) inflation of a circular flat membrane; (ii) inflation of a thin-walled cylindrical tube; (iii) inflation of a thin-walled spherical balloon. Four types of materials divided by increasing degree of compressibility are studied. The results indicate that volumetric deformations have a significant impact on both the limit pressure and the deformed shape. The proposed solutions represent benchmarks for developing new applications of compressible membranes made of polymeric foams and hydrogels, playing an increasingly important role in engineering technologies.

1. Introduction

Numerous applications in various fields of engineering involve the use of pressurized membranes. Because of the requirement to withstand large elastic deformations, membranes for technological applications are in most cases made of elastomers, polymeric foams, and hydrogels. Elastomeric membranes are widely used in electronics [1,2], soft robotics [3–5], dielectric systems [6,7], and aerodynamics [8]. Flexible polyurethane foam membranes are employed for robust capacitive pressure sensors [9], sound absorption in acoustic engineering [10], separation processes [11], and dye removal [12]. Hydrogel membranes find applications in medicine, environmental engineering, sensing, and energy storage [13]. Membrane modeling plays a major role also in biomechanics when dealing with soft tissues, such as fingertip pulp [14], arteries [15,16], and fetal membranes [17].

Given the growing interest in daily life and innovative engineering applications, recent studies have increasingly focused on modeling and utilizing hydrogels and foam membranes. Hong et al. [18] formulated a theory of the coupled mass transport and large deformations for polymeric gels in the framework of hyperelasticity. Ding et al. [19] presented equilibrium equations and implemented finite element analysis for inhomogeneous large deformations in temperature-sensitive hydrogels. Their investigation underscored the versatility of hydrogel membranes, demonstrating potential applications ranging from wound healing to soft robotics. Ahearne et al. [20] employed the indentation method to characterize the viscoelastic properties of alginate and agarose hydrogel circular membranes. These membranes, serving as models for soft biological tissues, have applications in tissue engineering and regenerative medicine, with potential use in constructing cornea, skin, and vascular tissues. Liu et al. [21] conducted a hyperelastic model study on instabilities in various polymeric gel membrane structures under large deformations. The biocompatibility of these membranes holds promise for applications in bioengineering and drug delivery. In [22], two-component soft cellular polyurethane membranes were utilized to reduce airflow in injured inflatable structures. The authors introduced a self-repairing membrane system, suggesting significant potential for extending functional integrity. Pientka et al. [23] employed a flexible closed-cell polystyrene foam membrane for effective biohydrogen separation. Elele et al. [24] conducted experiments on polymeric microfiltration membranes with pores, designed for water treatment. These membranes, experiencing large strains and temperature cycles during operation, require careful evaluation of their ability to withstand such elastic deformations.

In light of the preceding discussion, accurate nonlinear elastic models are increasingly essential for optimizing the potential of membranes made from novel materials like polymeric foams, hydrogels, and elastomers. Both polymeric foams and hydrogels exhibit significant compressibility, even in the small strain domain [25–27]. Consequently, accurate models for membrane technology should incorporate considerations for material compressibility. On the other hand, elastomers

* Corresponding author.
E-mail addresses: stefano.sirotti@unimore.it (S. Sirotti), matteo.pelliciari@unimore.it (M. Pelliciari), angelomarcello.tarantino@unimore.it (A.M. Tarantino).

https://doi.org/10.1016/j.ijmecsci.2024.109441
Received 24 January 2024; Received in revised form 29 May 2024; Accepted 30 May 2024
Available online 5 June 2024

are usually modeled in finite elasticity adopting the simplifying assumption of incompressibility, based on the observation that their bulk modulus is much larger than their shear modulus [28–31]. However, experiments have revealed that under large deformations, they may reach volume expansion up to 60% in simple tension and volume shrinkage of 15% during volumetric compression [32–35], depending on the composition of the rubber compound. Hence, it is necessary to consider the compressibility of elastomers as well, acknowledging the substantial volume changes observed under large deformations.

The prevailing models for hyperelastic membranes in the existing literature primarily rely on the assumption of incompressibility. For instance, the pioneering works on inflated circular membranes by Treloar [36] and Adkins and Rivlin [37] considered incompressible material models. Later works by Yang and Feng [38], DasGupta and Patil [39], and Chaudhuri and DasGupta [40] investigated the finite inflation of initially flat and pre-stretched circular membranes, assuming an isotropic and incompressible Mooney–Rivlin material model. Fu et al. [41], Ye et al. [42], and Mao et al. [43] analyzed the problem of bulging in short and long hyperelastic tubes made of incompressible material and inflated by internal pressure. Kyriakides and Chung [44,45] performed experiments to observe the formation and propagation of bulge in long cylindrical tubes under different axial loads. Alexander [46], Mangan and Destrade [47], and Kanner and Horgan [48] studied the equilibrium of pressurized spherical balloons composed of incompressible and isotropic nonlinear elastic materials. The focus was put on deriving analytical solutions for the investigation of the tensile instability during inflation. Liu et al. [49], Patil et al. [50], and Yang et al. [51] adopted incompressible neo-Hookean and Mooney–Rivlin laws to study the contact mechanics of inflated membranes against rigid and deformable substrates.

Some authors attempted to introduce material compressibility when modeling hyperelastic membranes. Firouzi and Żur [52] developed a total lagrangian finite element approach to solve equilibrium problems of compressible membranes. Pelliciari et al. [53] and Sirotti et al. [54] provided approximate analytical solutions for circular membranes made of compressible Mooney–Rivlin material. Chung et al. [55] derived analytical solutions for hollow circular cylinders and spheres under uniform internal pressure considering a particular compressible foam rubber described by the Blatz-Ko material model. Selvadurai and Suvorov [56] studied the inflation of poro-hyperelastic annuli adopting a compressible material described by a second-order polynomial strain energy density (SED).

The above works introduced volume changes in the mathematical formulations of hyperelastic membranes. However, they share the following limitations. Firstly, the adopted volumetric SED functions are designed for nearly incompressible elastomers, thus resulting inadequate for accurately describing the material response under large volume changes. Moreover, these functions fail to meet all the criteria for physical plausibility introduced by Doll and Schweizerhof [57] and later extended by Moerman et al. [58]. Therefore, they are considered inappropriate for providing a physically-based description of compressible materials. Secondly, the values of constitutive parameters describing volumetric deformations are not based on experimental measurements, leading to simulations that do not match real responses. The absence of an experimental foundation is a critical concern that compromises the capability of those models to faithfully represent the behavior of hyperelastic membranes. Lastly, the effect of compressibility on the mechanics of inflated membranes remains largely unexplored. In our previous works [53,54], we attempted to provide insights by varying parameters influencing compressibility, yet our efforts lacked a robust physical basis. This limitation stems from the fact that the modeling did not incorporate the separation of deviatoric and volumetric contributions. Without such a distinction, the drawn conclusions were of limited value. Additionally, inappropriate functions were used to describe volume changes and they were not based on experimental measurements. Consequently, there is an ongoing need to investigate the influence of compressibility on the overall response of membranes. The primary objective of the present work is to address the described limitations, offering a comprehensive analysis of the effect of compressibility in membrane problems.

The membrane model is developed by considering isotropic materials. The deviatoric–volumetric split of the SED is employed to separate the contribution of volumetric deformations. The volumetric SED adopted in this work was proposed in [35], and it was proven to be accurate in reproducing experimental responses of rubber-like materials subjected to both small and large volume changes. In order to study the behaviors of real compressible materials, the constitutive parameters of the volumetric SED are calibrated on experimental data of different types of elastomers, foams, and hydrogels. The equilibrium solutions for the following three cases are presented: inflation of a circular flat membrane, inflation of an infinite thin-walled cylindrical tube, and inflation of a thin-walled spherical balloon. The proposed solutions are then implemented in numerical codes. The effect of compressibility is analyzed and discussed by comparing these solutions with classical solutions of membrane problems under the assumption of material incompressibility.

The main innovations of the present work are summarized as follows. Firstly, in our previous studies on inflated membranes [53,54], the straightforward formulation for incorporating compressibility enabled us to derive a simple explicit relation for computing the transversal stretch of the membrane. However, when employing a more sophisticated SED that captures real behaviors, the relation for transversal stretch assumes an implicit form. This substantially raises the complexity of the involved differential equilibrium equations, necessitating a novel approach for obtaining a solution. Therefore, we provide an original numerical solution for the inflation of circular compressible membranes, implemented in MATLAB and made accessible to researchers. Secondly, we expand well-established elastic solutions for inflating thin-walled cylinders and spherical balloons, introducing an innovative aspect by incorporating compressibility with a grounded physical basis. Lastly, the role of compressibility in membrane problems is thoroughly investigated, considering real volumetric responses of elastomers, foams, and hydrogels. Significant effects on instabilities and limit pressure values are observed and discussed, emphasizing the importance of the proposed models in the development of technologies involving inflating rubber-like structures.

The paper is organized as follows. In Section 2 we summarize the main concepts of compressible hyperelasticity and we present the volumetric SED considered. In Section 3 we describe the materials considered and we fit the material parameters to experimental data. Section 4 reports the equilibrium solutions to the three membrane problems studied in this work. Results are presented and discussed in Section 5. Finally, conclusions are drawn in Section 6.

2. Compressibility in hyperelastic models

Elastic materials subjected to large deformations are typically studied in the framework of hyperelasticity, in which it is assumed the existence of a strain energy function W describing the material behavior [59,60]. In the case of isotropic materials [61], we write $W = W(I_1, I_2, I_3) = \tilde{W}(\lambda_1, \lambda_2, \lambda_3)$, where I_1, I_2 and I_3 are the principal strain invariants of the left Cauchy–Green deformation tensor $\mathbf{B} = \mathbf{F}\mathbf{F}^T$, being $\mathbf{F}$ the deformation gradient, and λ_1, λ_2 and λ_3 are the principal stretches. In the following, we focus on the case of W written as a function of the principal strain invariants. It goes without saying that the expressions can be easily written in terms of principal stretches.

The assumption of material incompressibility is based on the observation that, in linear elasticity, the bulk modulus of rubber-like materials is typically much larger than their shear modulus. In this case the deformation is isochoric, namely $J = \sqrt{I_3} = \det \mathbf{F} = \lambda_1\lambda_2\lambda_3 = 1$, and the SED is a function of I_1 and I_2 only.

On the other hand, in the case of compressible materials, the SED is written as a function of all three invariants. In this case, a convenient approach to separate the deviatoric (shape-changing) and hydrostatic (volume-changing) contributions is to use the split of the energy function [62,63]. The SED is written as

$$W = W_d\left(\bar{I}_1, \bar{I}_2\right) + W_h(J), \tag{1}$$

where $\bar{I}_1 = J^{-2/3} I_1$, $\bar{I}_2 = J^{-4/3} I_2$, and W_d and W_h are the terms responsible for shape and volume deformations, respectively. Hereinafter, $\bar{I}_1$ and $\bar{I}_2$ will be referred as deviatoric invariants.

The Cauchy stress tensor is expressed by $\mathbf{T} = \mathbf{T_d} + \sigma_h \mathbf{I}$, where $\mathbf{T_d}$ is the deviatoric part of the Cauchy stress, σ_h is the hydrostatic stress and $\mathbf{I}$ is the identity tensor. The hydrostatic stress reads [64]

$$\sigma_h = \frac{1}{3}\mathrm{tr}(\mathbf{T}) = \frac{dW_h(J)}{dJ}. \tag{2}$$

This relation allows an independent characterization of the volumetric SED, W_h, from experimental tests involving volumetric deformations. In particular, the relation between the stress and W_h in simple tension becomes

$$\frac{1}{3}\sigma_1 = \sigma_h = \frac{dW_h(J)}{dJ}, \tag{3}$$

where σ_1 is the principal Cauchy stress in the longitudinal direction. The two lateral principal stresses are zero ($\sigma_2 = \sigma_3 = 0$).

2.1. The strain energy function

The complete description of the response of a compressible material requires the choice of both deviatoric and volumetric functions W_d and W_h. In this regard, in work [35] we carried out experiments on elastomers and concluded that: (1) among the numerous forms of W_d available in the literature (see, e.g., [65–68]), the Yeoh–Fleming model [69] seemed to give the best compromise between simplicity and accuracy for both small and large strains; (2) there was a lack of accurate volumetric SED functions for rubber-like materials, therefore we proposed a new form of W_h. Given the above, in the present work we adopt the Yeoh–Fleming model and the volumetric strain energy proposed in [35] as W_d and W_h, respectively.

The function proposed by Yeoh and Fleming reads

$$W_d\left(\bar{I}_1\right) = \frac{A}{B}\left(I_m - 3\right)\left(1 - e^{-B(\bar{I}_1 - 3)/(I_m - 3)}\right) - C_{10}\left(I_m - 3\right)\ln\left(1 - \frac{\bar{I}_1 - 3}{I_m - 3}\right), \tag{4}$$

being A, B, C_{10} and I_m the constitutive parameters of the model. The volumetric SED proposed by Pelliciari et al. [35] is expressed by $W_h(J) = \kappa\left[H(1-J)\Psi_c + H(J-1)\Psi_t\right]$, where κ is the bulk modulus and H is the Heaviside step function. Functions Ψ_c and Ψ_t control respectively the responses for volume shrinkage and expansion, and are defined as

$$\begin{aligned}
\Psi_c(J) &= \frac{1}{\alpha_1 + \alpha_2 - \alpha_3}\left[\left(J + \frac{J^{\alpha_1+1}}{\alpha_1+1} + \frac{J^{-(\alpha_2-1)}}{\alpha_2-1} - \frac{J^{\alpha_3+1}}{\alpha_3+1}\right)\right. \\
&\quad \left. - \left(1 + \frac{1}{\alpha_1+1} + \frac{1}{\alpha_2-1} - \frac{1}{\alpha_3+1}\right)\right], \\
\Psi_t(J) &= (1-q)\left[\frac{\beta_2 e^{\beta_1(J-1)} + \beta_1 e^{-\beta_2(J-1)}}{\beta_1\beta_2(\beta_1+\beta_2)} - \frac{1}{\beta_1\beta_2}\right] \\
&\quad + q\beta_3^2 \ln\left(\cosh\left(\frac{J-1}{\beta_3}\right)\right).
\end{aligned} \tag{5}$$

The model involves seven parameters in addition to the bulk modulus: α_1, α_2 and α_3 that control the response in shrinkage; β_1, β_2, β_3 and q that control the response in expansion. The use of the Heaviside step function allows an independent control of the two behaviors. The hydrostatic stress is derived using Eq. (2).

Thin membranes are not capable of sustaining compressive stresses, therefore they admit only tensile stress states. Consequently, the hydrostatic stress in such problems is always positive, which means that the volume is only expanding ($J > 0$). Hence, from now on, in the energy we consider only the term Ψ_t related to volume expansion and we neglect the term Ψ_c responsible for volume contraction. Namely,

$$W_h(J) = \kappa\,\Psi_t(J), \quad \sigma_h(J) = \kappa\,\frac{d\Psi_t}{dJ}. \tag{6}$$

As a consequence, the constitutive parameters of the volumetric SED reduce to four: β_1, β_2, β_3 and q.

The complete response of the compressible material is described by the combined SED, $W\left(\bar{I}_1, J\right) = W_d\left(\bar{I}_1\right) + W_h(J)$, where W_d and W_h are expressed respectively by Eqs. (4) and (6).

3. Materials and parameter fitting

In this section we describe the materials considered in this study, which are characterized by four different degrees of compressibility. For each material, we present the experimental data obtained from simple tension tests. The parameters of the strain energy function are fitted to the experimental responses. In the parameter fitting, both the cases of compressible and incompressible models are considered. This is done because, in the following sections, we will present a comparison between compressible and incompressible responses in membrane problems.

3.1. Description of the materials

In order to provide a comprehensive description of the effect of compressibility, we define the following four types of materials: (I) materials that are nearly incompressible for any magnitude of applied strain; (II) materials that are nearly incompressible for small strains and become compressible for large strains; (III) materials that are compressible for both small and large strains; (IV) auxetic materials. As type I materials, we consider the NR (natural rubber) and silicone analyzed in the work [35]. As type II materials, we consider the EPDM (ethylene propylene diene monomer) and NBR (nitrile butadiene rubber) from work [35]. As type III materials, we study the polymeric foam and the hydrogel tested in works [70,71], respectively. Finally, as a type IV material, we consider the foam analyzed in [72].

We remark that our purpose is to shed light on the role of material compressibility in thin membranes. We are aware that, for materials of type III and IV, the assumption of incompressibility is inappropriate from a theoretical standpoint. However, our goal is to study the differences between compressible and incompressible models, which are emphasized when the material is characterized by a marked compressibility. We also note that we consider only data from simple tension tests because our primary objective is not to conduct an accurate characterization of the response of the materials to biaxial stress states, which would necessitate data from experiments such as biaxial, equibiaxial or pure shear tests [73]. Instead, our focus is on highlighting the role of volumetric deformations in membranes. Thus, calibrating material response solely through simple tension testing suffices to highlight its influence and distinguish differences from incompressible and compressible models.

The experimental data of the aforementioned materials are represented in Fig. 1. For the sake of clarity, the longitudinal and hydrostatic stress of types III and IV materials are normalized with respect to the following values of Young modulus: $E = 650$ kPa for the foam, $E = 1.9$ kPa for the hydrogel and $E = 15$ kPa for the auxetic foam. The black curves in Figs. 1(d) and 1(e) represent the incompressible behavior, expressed by $\lambda_y = 1/\sqrt{\lambda_x}$. From Fig. 1(d), we notice that both NR and silicone are nearly incompressible throughout the experiment. EPDM and NBR are almost incompressible only in the region of small strains. Figs. 1(e) and 1(f) show that the foam from [70] and the hydrogel are compressible in the entire range of deformation, while the foam from [72] exhibits an auxetic behavior.

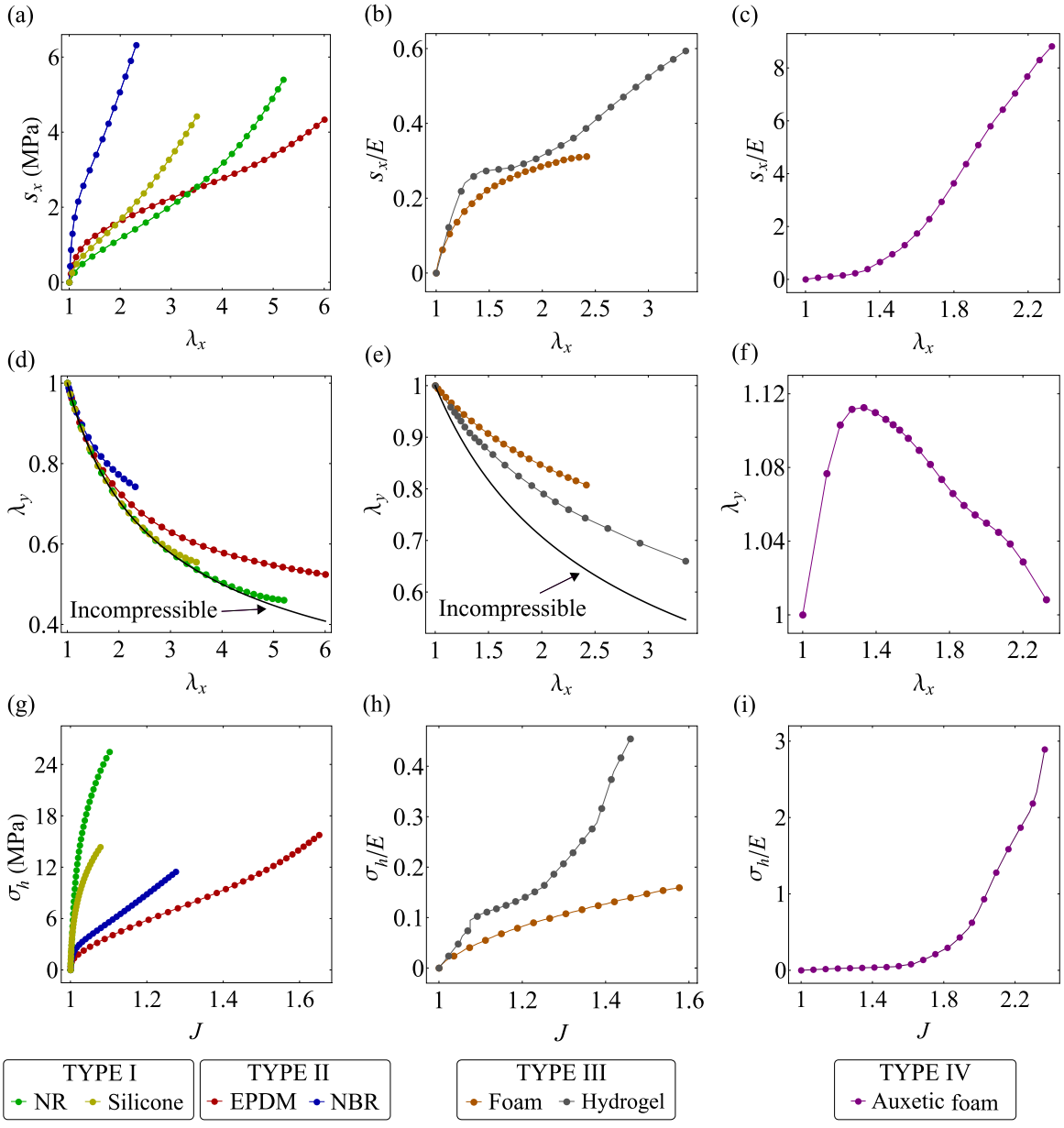

Fig. 1. Experimental data from simple tension tests: (a)–(c) nominal stress vs. stretch; (d)–(f) lateral vs. longitudinal stretches; (g)–(i) hydrostatic stress vs. volume variation. Details on the experiments on elastomers can be found in [35]. The data of foam, hydrogel and auxetic foam were digitized respectively from Blatz and Ko [70], Urayama et al. [71], and Choi and Lakes [72]. The values of Young modulus are $E = 650$ kPa for the foam, $E = 1.9$ kPa for the hydrogel and $E = 15$ kPa for the auxetic foam.

3.2. Model fitting

The constitutive parameters for NR, silicone, EPDM and NBR for both compressible and incompressible models had already been fitted in [35]. In the present work, we consider such values of the model parameters. Regarding the other materials, the parameters are fitted as described in the following.

The equilibrium solution in simple tension is summarized in Appendix A, in the cases of both incompressible and compressible models. For incompressible models, the stress vs. strain relation is given by Eq. (A.3). This relation was fitted to the longitudinal stress vs. stretch data using function *FindFit* in Wolfram Mathematica. The optimal parameters of all the materials analyzed, including the elastomers, are reported in Table B.2.

For compressible models, the fitting was performed in two steps. Firstly we calibrated the parameters of the volumetric SED (W_h), successively the parameters of the deviatoric SED (W_d). The procedure was the following:

(1) For each material, the bulk modulus κ was calibrated from the initial slope of the σ_h vs. J data from simple tension tests. Then, the hydrostatic stress σ_h was fitted to the entire experimental σ_h vs. J curve. In this way, volumetric model parameters β_1, β_2, β_3 and q were calibrated. This fitting was performed by means of function *FindFit* in Wolfram Mathematica.
(2) The equilibrium solution in simple tension, described by Eqs. (A.1) and (A.2), was fitted to the experimental data. In particular, the above equations were written in a MATLAB code. Function *fsolve* was employed to numerically solve the implicit equation between

longitudinal and lateral stretches, Eq. (A.1). The stress vs. stretch relation, expressed by Eq. (A.2), was fitted to the s_x vs. λ_x data. This was done by considering as objective function the sum of squared residuals between analytical and experimental stress vs. stretch curves, and performing the optimization in MATLAB with function *fmincon*.

The optimal values of parameters for the compressible models are given in Table B.3. We remark that, as commonly happens in nonlinear optimization problems, multiple sets of parameters may yield satisfactory fitting solutions. However, the advantage of splitting the deviatoric and volumetric contributions is that the parameters involved in W_h were calibrated independently. Subsequently, the remaining parameters of W_d were calibrated. Furthermore, all parameters have physical meanings, which guides us in obtaining reasonable values.

Fig. 2 shows the curves obtained from the incompressible and compressible models. Since the elastomers were already analyzed in [35], we report only the curves for materials of types III and IV (foam, hydrogel and auxetic foam). The fitting curves for elastomers, namely materials of types I and II, can be found in Figs. 11 and 13 in [35]. Figs. 2(a) and 2(b) show the normalized stress vs. stretch curves for material types III and IV with incompressible model, respectively. On the other hand, Figs. 2(c) and 2(d) show the normalized stress vs. stretch curves in the case of compressible model. We observe that both incompressible and compressible models give accurate predictions of the tensile stress response of the materials analyzed. For the compressible model, Figs. 2(e) and 2(f) show that the description of the lateral stretch is accurate, as well as the hydrostatic stress as a function of the volume change (Figs. 2(g) and 2(h)).

Introducing the hypothesis of small strains, the equilibrium equations in simple tension can be linearized to obtain the following expressions of the elastic constants of linear elasticity:

$$E = \frac{18k\left(A + C_{10}\right)}{2\left(A + C_{10}\right) + 3k}, \qquad \nu = \frac{3k - 4\left(A + C_{10}\right)}{4\left(A + C_{10}\right) + 6k}. \tag{7}$$

The values of the Poisson's ratio ν for each material considered are reported in Table B.3. The values of ν for materials of type I and II are very close to 0.5, proving they are almost incompressible at small strains. On the contrary, materials of type III have a Poisson's ratio of 0.326 and 0.332, namely they exhibit significant volume changes even at small strains. Finally, type IV material has a negative value of Poisson's ratio, showing the distinctive behavior of auxetic materials of expanding laterally when subjected to longitudinal traction.

4. Equilibrium solutions for inflated membranes

In this section we present the three benchmark problems considered in this work: (1) inflation of a circular flat membrane; (2) inflation of an infinitely long thin-walled cylindrical tube; (3) inflation of a thin-walled spherical balloon. A schematic representation of the three problems is reported in Fig. 3. We present the equilibrium solutions for a generic isotropic, compressible, hyperelastic material described by a strain energy function W. We develop the solutions for a SED written as a function of the principal strain invariants, $W = W\left(I_1, I_2, I_3\right)$, since this is the case of most hyperelastic models. In this circumstance, the derivatives with respect to the principal stretches are computed with the chain rule:

$$\frac{\partial W}{\partial \lambda_i} = 2\lambda_i\left(w_1 + \left(\lambda_j^2 + \lambda_k^2\right)w_2 + \lambda_j^2\lambda_k^2 w_3\right), \qquad i,j,k = 1,2,3 \tag{8}$$

where $w_j = \partial W/\partial I_j$, with $j = 1,2,3$. In case of the combined SED, $W\left(\bar{I}_1, J\right)$, the derivatives of W with respect to the principal strain invariants I_1, I_2 and I_3 are computed with the chain rule. To study the effect of compressibility, the solutions for compressible membranes presented in this section will be compared with the solutions for incompressible membranes, which are recalled in Appendix D.

4.1. Circular flat membrane

We consider a circular flat membrane with radius L and thickness H (see Fig. 3(a)). We define a cylindrical coordinate system (R, Θ, Z) with origin in the central point of the membrane. The membrane is inflated under a uniform lateral pressure p and we assume the deformation is axisymmetric. A generic material point $P \equiv (R, \Theta, 0)$ moves to P', with coordinates (r, Θ, z). The principal directions of stretch correspond to the meridians, the latitudinal lines, and the normal to the deformed surface. The principal stretches are $\lambda_1 = \sqrt{r'^2 + z'^2}$, $\lambda_2 = r/R$, and $\lambda_3 = h/H$, where h is the thickness of the membrane in the deformed configuration and the prime denotes differentiation with respect to R. The principal Cauchy stresses are given by

$$\sigma_i = \frac{1}{\lambda_j\lambda_k}\frac{\partial W}{\partial \lambda_i}, \quad i,j,k = 1,2,3. \tag{9}$$

The membrane assumption $\sigma_3 = \partial W/\partial\lambda_3 = 0$ leads to the following relation for λ_3:

$$G\left(\lambda_1, \lambda_2, \lambda_3\right) = \frac{\partial W}{\partial \lambda_3} = w_1 + \left(\lambda_1^2 + \lambda_2^2\right)w_2 + \lambda_1^2\lambda_2^2 w_3 = 0, \tag{10}$$

which allows to compute the transversal stretch λ_3 for each pair $\left(\lambda_1, \lambda_2\right)$.

Eq. (10) yields an explicit expression for λ_3 only in specific cases of limited practical interest. Indeed, an explicit expression for λ_3 can be obtained only for simple material models and without splitting the SED function into deviatoric and hydrostatic contributions. For instance, in [53,54] we modeled compressibility by adding the Charlet–Geymonat function [74] to a two-term Mooney–Rivlin model, deriving an explicit relation for λ_3. However, due to its mathematical simplicity, this model fails to accurately represent the true response of elastomers to large volume changes. Moreover, without splitting the SED function, both deviatoric and hydrostatic terms contribute to the response to volume deformations, making it impossible to characterize the volumetric behavior of the material. Therefore, we derive the solution for the most general case, where Eq. (10) is implicit and the computation of transversal stretch λ_3 requires numerical methods.

The principal stress resultants per unit length are computed as $T_i = \lambda_3 H\sigma_i$, with $i = 1,2$. The equilibrium equations in radial and normal directions read

$$\begin{aligned} &\frac{dT_1}{dr} + \frac{1}{r}(T_1 - T_2) = 0, \\ &K_1T_1 + K_2T_2 = p, \end{aligned} \tag{11}$$

where $K_1 = (\lambda_1'\eta - \lambda_1\eta')/(\lambda_1^2\sqrt{\lambda_1^2 - \eta^2})$ and $K_2 = (\sqrt{\lambda_1^2 - \eta^2})/(\lambda_1\lambda_2 R)$ are the principal curvatures, with $\eta = r'$. Substituting the expressions for T_1, T_2, K_1, and K_2 into Eq. (11), the following system of differential equations is obtained:

$$\begin{aligned} \lambda_1' &= \frac{\xi_0 + \xi_1 w_1 + \xi_2 w_2 + \xi_3 w_3}{w_1 + w_2\xi_4 + w_3\xi_5 + \frac{\partial w_1}{\partial\lambda_1}\lambda_1 + \frac{\partial w_2}{\partial\lambda_1}\lambda_1\lambda_2^2 + \frac{\partial w_2}{\partial\lambda_1}\lambda_1\lambda_3^2 + \frac{\partial w_3}{\partial\lambda_1}\lambda_1\lambda_3^2\lambda_2^2}, \\ \lambda_2' &= \frac{\eta - \lambda_2}{R}, \\ \eta' &= \frac{\eta\lambda_1'}{\lambda_1} + \frac{2\zeta_1\lambda_2\left(\lambda_1^2 - \eta^2\right) - \phi\lambda_2\lambda_1^2\sqrt{\lambda_1^2 - \eta^2}}{2\zeta_2\lambda_1^2 R}, \end{aligned} \tag{12}$$

where $\phi = pR/H$ and, for the sake of clarity, the following quantities were defined:

$$\begin{aligned} \xi_0 &= \lambda_1^2\frac{\partial w_1}{\partial\lambda_2}\left(\lambda_2 - \eta\right) + \lambda_1^2\frac{\partial w_2}{\partial\lambda_2}\left(-\eta\lambda_2^2 - \eta\lambda_3^2 + \lambda_2^3 + \lambda_2^2\lambda_2\right) + \lambda_1^2\lambda_3^2\lambda_2^2\frac{\partial w_3}{\partial\lambda_2}\left(\lambda_2 - \eta\right), \\ \xi_1 &= \eta\lambda_2 - \lambda_1^2, \\ \xi_2 &= -2\frac{\partial\lambda_3}{\partial\lambda_2}\eta\lambda_3\lambda_1^2 + 2\frac{\partial\lambda_3}{\partial\lambda_2}\lambda_2\lambda_3\lambda_1^2 - \eta\lambda_2\lambda_1^2 + \eta\lambda_2\lambda_3^2 + \lambda_2^2\lambda_1^2 - \lambda_3^2\lambda_1^2, \\ \xi_3 &= -2\frac{\partial\lambda_3}{\partial\lambda_2}\eta\lambda_1^2\lambda_3\lambda_2^2 + 2\frac{\partial\lambda_3}{\partial\lambda_2}\lambda_1^2\lambda_3\lambda_2^3 - \eta\lambda_1^2\lambda_3^2\lambda_2 + \lambda_1^2\lambda_3^2\lambda_2^2, \end{aligned} \tag{13}$$

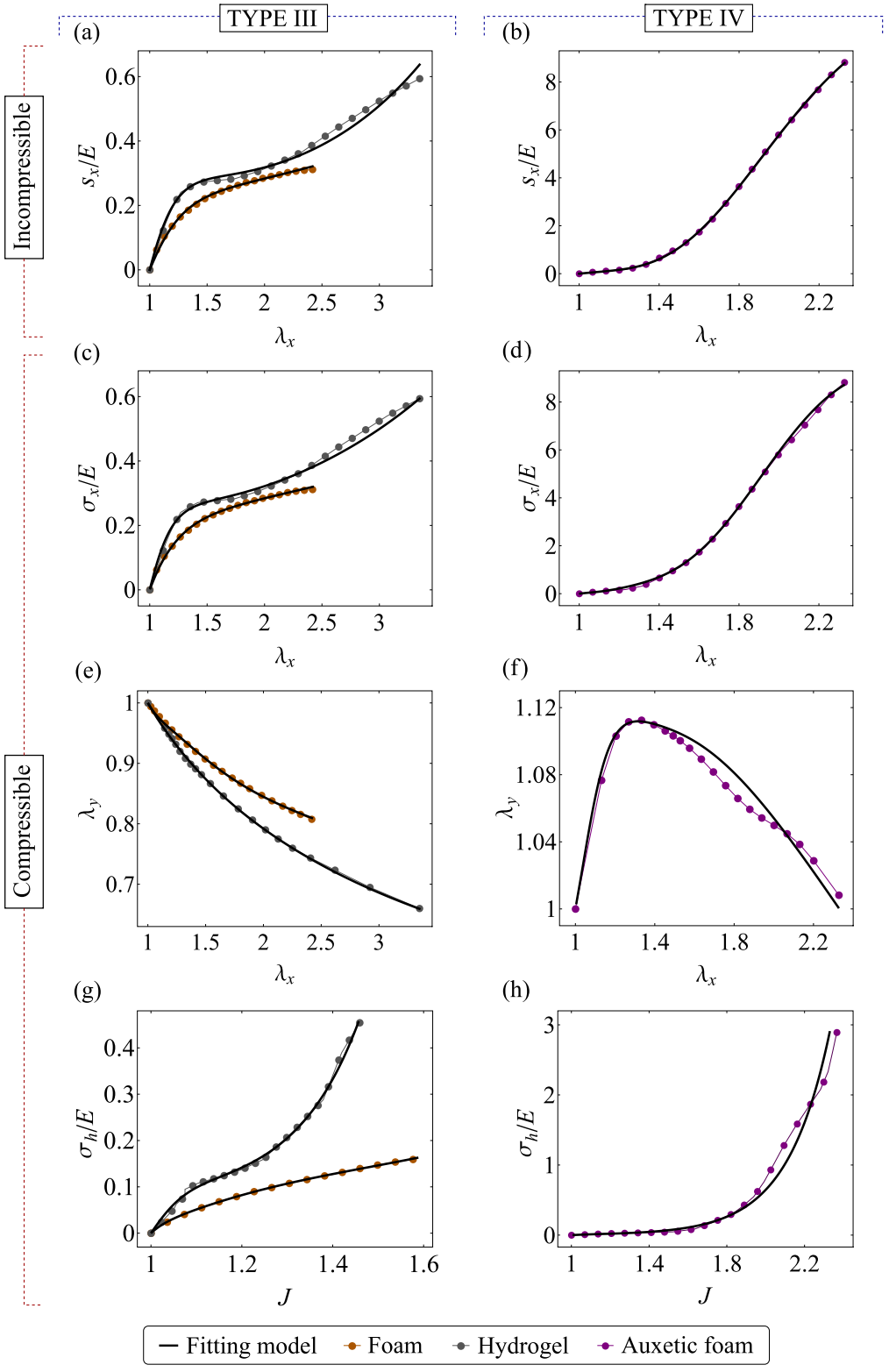

Fig. 2. Results of model fitting in case of incompressible and compressible models for material types III and IV. Stress vs. stretch plots for incompressible, (a) and (b), and compressible models, (c) and (d). For the compressible model, the plots of λ_y vs. λ_x and σ_h/E vs. J are shown respectively in (e) and (f), and (g) and (h). Solid and dotted lines represent model fitting and experimental data, respectively. The model fitting for elastomers, namely material types I and II, is shown in Figs. 11 and 13 in [35].

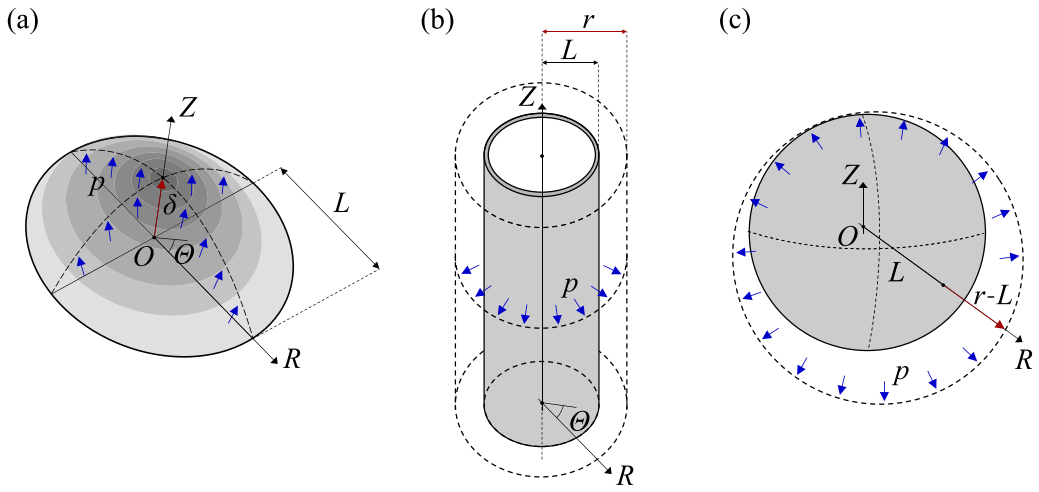

Fig. 3. Schematic representation of the three membrane problems analyzed in the present work: (a) inflation of a circular flat membrane; (b) inflation of an infinitely long thin-walled cylindrical tube; (c) inflation of a thin-walled spherical balloon.

$$\xi_4 = 2\frac{\partial\lambda_3}{\partial\lambda_1}\lambda_1\lambda_3 + \lambda_2^2 + \lambda_3^2,$$
$$\xi_5 = 2\frac{\partial\lambda_3}{\partial\lambda_1}\lambda_1\lambda_3\lambda_2^2 + \lambda_3^2\lambda_2^2,$$
$$\zeta_1 = w_1 + \lambda_1^2 w_2 + \lambda_3^2\left(\lambda_1^2 w_3 + w_2\right),$$
$$\zeta_2 = w_1 + \lambda_2^2 w_2 + \lambda_3^2\left(\lambda_2^2 w_3 + w_2\right).$$

The derivatives of λ_3 with respect to λ_1 and λ_2 can only be computed numerically by means of the implicit function theorem, namely

$$\frac{\partial\lambda_3}{\partial\lambda_1} = -\frac{\partial G/\partial\lambda_1}{\partial G/\partial\lambda_3}, \quad \frac{\partial\lambda_3}{\partial\lambda_2} = -\frac{\partial G/\partial\lambda_2}{\partial G/\partial\lambda_3}. \tag{14}$$

The derivatives of w_1, w_2 and w_3 with respect to λ_1 and λ_2 are computed with the chain rule

$$\frac{\partial w_i}{\partial\lambda_j} = \sum_{k=1}^{3}\frac{\partial w_i}{\partial I_k}\left(\frac{\partial I_k}{\partial\lambda_j} + \frac{\partial I_k}{\partial\lambda_3}\frac{\partial\lambda_3}{\partial\lambda_j}\right), \qquad i = 1,2,3 \quad \text{and} \quad j = 1,2. \tag{15}$$

The system of equilibrium equations (Eq. (12)) represents an initial value problem that must be integrated along the radius of the membrane, with the additional condition $\lambda_2(L) = 1$ that must be satisfied at the outer boundary. The system requires a numerical integration, which was performed in MATLAB by means of function *ode45*. The radius was discretized in steps $dR = L/1000$ and the integration was performed starting from the pole, with initial condition $\lambda_1 = \lambda_2 = \eta = \lambda_0$, to the outer boundary, where the additional condition $\lambda_2(L) = 1$ must be satisfied. The steps are the following: (i) the initial condition at the pole λ_0 and a guess value p_0 for the pressure are set; (ii) the corresponding transversal stretch λ_3 is computed solving numerically Eq. (10) with $\lambda_1 = \lambda_2 = \lambda_0$; (iii) quantities $\partial\lambda_3/\partial\lambda_1$, $\partial\lambda_3/\partial\lambda_2$, $\partial w_1/\partial\lambda_1$, $\partial w_1/\partial\lambda_2$, $\partial w_2/\partial\lambda_1$, $\partial w_2/\partial\lambda_2$, $\partial w_3/\partial\lambda_1$ and $\partial w_3/\partial\lambda_2$ are computed from Eqs. (14) and (15); (iv) the values of λ_1, λ_2 and η at the next point of the domain are computed from Eq. (12); (v) steps (ii), (iii) and (iv) are repeated for each point along the domain until $\lambda_2 = 1$. The value of R at which $\lambda_2 = 1$ is denoted by R^*; (vi) in general, the initial guess value p_0 will be different from the correct pressure p and thus R^* will be different from L. However, system (12) is invariant when a scaling factor is multiplied to R [75]. Hence we choose $\gamma = L/R^*$ as scaling factor and we compute the correct value of pressure as $p_1 = p_0/\gamma = p_0 R^*/L$; (vii) perform again the numerical integration with the correct value p_1, obtain the correct stretches profiles λ_1 and λ_2 and the deformed coordinates r and z; (viii) repeat this procedure for different initial conditions λ_0 to derive the entire pressure curve. The solution obtained with this procedure for compressible materials was validated by means of finite element (FE) simulations carried out on COMSOL, described in Appendix C.

For each material, we had to define the maximum stretch $\lambda_{0,max}$ to apply at the pole as initial condition. This choice required attention in order to avoid a level of deformation higher than the one attained during the parameters calibration. Since the parameters were calibrated on uniaxial tensile tests, a natural choice for the value of $\lambda_{0,max}$ would be the maximum longitudinal stretch $\lambda_{x,max}$ reached in the experimental tests. However, since membrane inflation is a biaxial problem, the overall strain state would differ substantially from the case of uniaxial tension. Therefore, a global measure of deformation seems more appropriate. To this aim, we assumed the first deviatoric invariant $\bar{I}_1$ as measure of deformation. Thereby, we set $\lambda_{0,max}$ so that $\bar{I}_1$ computed at the pole of the membrane matched the value of $\bar{I}_1$ at the end of the uniaxial tensile test. The choice of $\bar{I}_1$ is supported by the observation that it is the only independent variable of the Yeoh–Fleming model. This approach guarantees that the range of reliability of the fitted model parameters is never exceeded. The maximum stretch $\lambda_{0,max}$ determined with this approach is adopted also for the inflation of the cylindrical tube and the spherical balloon, described in the following.

4.2. Infinite thin-walled cylindrical tube

We now consider the inflation of an infinitely long, thin-walled cylindrical tube. In the undeformed configuration, the tube has uniform thickness H and radius L (see Fig. 3(b)). During inflation, we assume that the axial stretch at infinity is kept fixed to unity and the deformed configuration is axially symmetric. The deformed radius can remain constant (uniform solution) or vary along the axial direction (bifurcated state). During the uniform solution, also called primary state, the tube expands uniformly in the lateral direction. The axial stretch remains equal to unity over the whole domain and the length of the tube is fixed, whereas the axial force acting along the tube varies with pressure in order to keep the length fixed. Under these conditions, bifurcation can take place even when the pressure increases monotonically [76]. In the bifurcated state, the axial stretch varies along the bulge profile but it tends to unity moving away from it. Following the work by Fu et al. [41], we briefly present the uniform solution and the bifurcation condition for this problem.

A generic material point $P \equiv (L, \Theta, Z)$ is mapped into P', with coordinates $(r(Z), \Theta, z(Z))$. The meridional, latitudinal, and normal directions are the principal directions of strain, and the principal stretches read $\lambda_1 = \sqrt{r'^2 + z'^2}$, $\lambda_2 = r/L$, and $\lambda_3 = h/H$. Here the prime denotes differentiation with respect to Z. The principal Cauchy stresses are given by Eq. (9). The membrane assumption $\sigma_3 = \partial W/\partial\lambda_3 = 0$ gives

again Eq. (10), which relates the transversal stretch λ_3 to λ_1 and λ_2. The equilibrium equations are [77]

$$\frac{1}{h}\frac{d\left(h\sigma_1\right)}{dZ}+\frac{r'}{r}(\sigma_1-\sigma_2)=0, \tag{16}$$

$$\frac{\sigma_1\left(r''z'-r'z''\right)}{\left(r'^2+z'^2\right)^{\frac{3}{2}}}-\frac{\sigma_2 z'}{r\left(r'^2+z'^2\right)^{\frac{1}{2}}}+\frac{p}{h}=0. \tag{17}$$

We define the normalized pressure $\bar{p}=pL/H$ and assume that the tube remains uniform far away from the origin with a constant radius r_∞. Thus, as $Z\to\pm\infty$, we have: $r\to r_\infty$, $r'\to 0$, $r''\to 0$, $z\to Z$, $z'\to 1$, $\lambda_1\to 1$, and $\lambda_2\to r_\infty/L$. The pressure p is determined from Eq. (17) as

$$\bar{p}=\frac{1}{\lambda_{2,\infty}}\frac{\partial W}{\partial\lambda_2}^{(\infty)}, \tag{18}$$

where the superscript (∞) means evaluation at $\lambda_1=1$ and $\lambda_2=r_\infty/L=\lambda_{2,\infty}$. Eq. (18) determines the $\bar{p}$ vs. $\lambda_{2,\infty}$ curve in case of uniform inflation.

The numerical solution was obtained by defining in MATLAB a vector of values of $\lambda_{2,\infty}$, ranging from 1 to $\lambda_{0,max}$. For each value of $\lambda_{2,\infty}$, Eq. (10) is expressed as $G\left(1,\lambda_{2,\infty},\lambda_3\right)=0$ and it was numerically solved using MATLAB function *fsolve*. The solution provided the value of transversal stretch λ_3 that satisfies the membrane assumption. The obtained value of λ_3 was substituted into Eq. (18) to compute the corresponding pressure.

As $\lambda_{2,\infty}$ increases the uniform solution may reach a bifurcation point after which a bulging/necking of the tube takes place. The bifurcation condition reads [41]

$$\lambda_{2,\infty}\left(\frac{\partial W}{\partial\lambda_2}^{(\infty)}-\frac{\partial^2 W}{\partial\lambda_2\partial\lambda_1}^{(\infty)}\right)^2+\frac{\partial^2 W}{\partial\lambda_1^2}^{(\infty)}\left(\frac{\partial W}{\partial\lambda_2}^{(\infty)}-\lambda_{2,\infty}\frac{\partial^2 W}{\partial\lambda_2^2}^{(\infty)}\right)=0. \tag{19}$$

When computing the second derivatives $\partial^2 W/\partial\lambda_i\partial\lambda_j$, the dependence of λ_3 on λ_1 and λ_2 must be taken into account, writing

$$\frac{\partial^2 W}{\partial\lambda_i\partial\lambda_j}=\sum_{k=1}^{3}\frac{\partial^2 W}{\partial\lambda_i\partial I_k}\left(\frac{\partial I_k}{\partial\lambda_j}+\frac{\partial I_k}{\partial\lambda_3}\frac{\partial\lambda_3}{\partial\lambda_j}\right),\qquad i,j=1,2 \tag{20}$$

where $\partial\lambda_3/\partial\lambda_j$ are given by Eq. (14). The value of $\lambda_{2,\infty}=r_\infty/L$ satisfying Eq. (19) determines the critical radius that leads to the bifurcated solution. The bifurcation point was determined using MATLAB. Eq. (19) was solved by means of function *fzero*, which searched iteratively the solution starting from an initial value of $\lambda_{2,\infty}$. For each iteration, before computing Eq. (19), the corresponding value λ_3 was determined solving $G\left(1,\lambda_{2,\infty},\lambda_3\right)=0$ with function *fsolve* and the derivatives of W with respect to the stretches were computed.

4.3. Thin-walled spherical balloon

We consider a thin-walled spherical balloon of initial radius L and thickness H (see Fig. 3(c)). We assume that during the inflation the balloon retains its spherical shape. Due to the symmetry of the problem, each point is subjected to equibiaxial extension. The deformation is homogeneous and the principal stretches are $\lambda_1=\lambda_2=\lambda=r/L$ and $\lambda_3=h/H$, where r and h are respectively the deformed radius and thickness. The equilibrium equations, Eq. (11), reduce to [78]

$$\sigma=\frac{pr}{2h}, \tag{21}$$

where σ is the principal Cauchy stress acting in the deformed plane. Substituting Eq. (9) into Eq. (21), we obtain the relation for the normalized pressure $\bar{p}=pL/H$

$$\bar{p}=\frac{4}{\lambda}\left[w_1+\left(\lambda^2+\lambda_3^2\right)w_2+\lambda^2\lambda_3^2 w_3\right]. \tag{22}$$

The membrane assumption, defined by Eq. (10), reduces to

$$w_1+2\lambda^2 w_2+\lambda^4 w_3=0. \tag{23}$$

This equation allows us to compute the transversal stretch λ_3 for each value of λ. In particular, a list of values for λ ranging from 1 to $\lambda_{0,max}$ was defined and the above equation was numerically solved using function *fsolve* in MATLAB. The numerical value of λ_3 was then substituted into Eq. (22) to compute the corresponding value of pressure.

For increasing values of λ, the uniform spherical solution can bifurcate into an asymmetrical pear-shaped configuration. However, Haughton and Ogden [79] showed that the bifurcation always occurs after the maximum pressure is reached. For this reason, we did not focus on the bifurcation condition for spherical balloons.

5. Results

In this section we compare the results of incompressible and compressible models in the inflation of circular membranes, thin-walled cylindrical tubes and spherical balloons. We remark that the goal of this section is to analyze and discuss the effect of compressibility on the response of thin membranes. To this aim, we consider the constitutive parameters calibrated in Section 3.2 from simple tension tests. The parameters of incompressible and compressible models gave nearly equal responses in terms of stress vs. stretch in simple tension (see Fig. 2). In the following, we present the corresponding results for the three membrane problems described above. Eventual differences in the response are to be attributed to compressibility and will be discussed in detail.

5.1. Circular flat membrane

For each material, the numerical solution for flat circular membranes under inflation was derived according to Section 4.1. The results in terms of pressure vs. deflection curve, deformed shape and pressure vs. volume curve are presented in Fig. 4 for elastomers (types I and II), and Fig. 5 for material types III and IV. The deformed shapes displayed in the second column of the above figures are related to the configuration at the maximum pressure $\bar{p}$ from the compressible model.

As expected, from Fig. 4 we notice that incompressible and compressible models for materials of type I give very similar responses. This is due to the fact that volume deformations are small and thus the contribution of the volumetric strain energy is almost unnoticeable. However, materials of type II show sensible discrepancies between incompressible and compressible solutions. In case of EPDM, the pressure vs. deflection curve exhibits a limit pressure followed by a softening branch. The effect of compressibility occurs particularly near the limit point, which is the point of most interest from a practical standpoint. On the other hand, NBR shows a monotonic trend in the pressure vs. deflection curve, and the effect of compressibility increases as the deformation increases.

Another comparison may be done in terms of deformed shape corresponding to the maximum pressure. In practical applications, membranes are generally inflated in pressure control, namely by applying increasing internal pressure. Hence, for a given value of pressure, the deflection, if not the entire deformed shape, is of much interest. In view of this, Figs. 4(h) and 4(m) display the deformed shapes at maximum pressure. It is clear that, despite the error in terms of pressure is modest, a significant discrepancy in the deformed shape occurs when a wrong assumption on the compressibility of the material is made. This means that large errors in the prediction of the deformed shapes can be expected when modeling type II materials with the assumption of incompressibility. This consideration plays a crucial role in applications such as contact mechanics, where accurate predictions of the deformed shapes are required.

In a few cases, the inflation may be performed in volume control. Hence, the third column of Figs. 4 and 5 shows the pressure vs. volume curves. We notice a direct correspondence between the pressure vs. volume curves and the pressure vs. deflection curves for all the materials considered. Regarding type II materials, Figs. 4(i) and 4(n)

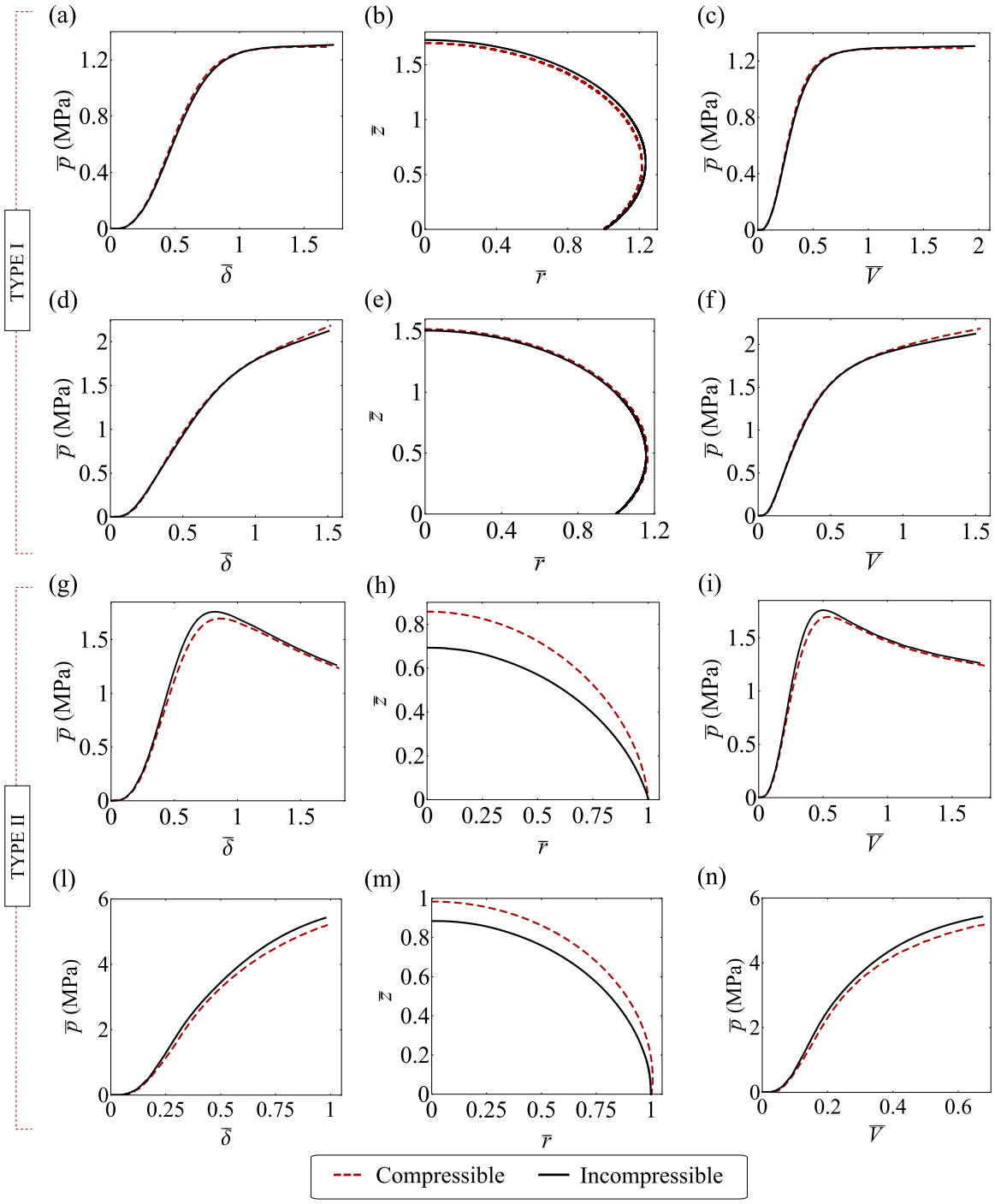

Fig. 4. Inflation of a circular flat membrane. The results are shown for (a)–(c) NR, (d)–(f) silicone, (g)–(i) EPDM, (l)–(n) NBR, in terms of normalized pressure $\bar{p} = pL/H$ vs. deflection $\bar{\delta} = \delta/L$ curve, normalized deformed shapes ($\bar{r} = r/L$, $\bar{z} = z/L$) and normalized pressure $\bar{p} = pL/H$ vs. volume $\bar{V} = V/(\pi L^3)$ curve. For each material, the deformed shape corresponds to the value of maximum pressure on the compressible curves.

show that for a given volume, the incompressible model gives a good prediction of the pressure. Hence, in case of inflation in volume control, the assumption of incompressibility remains acceptable for type II materials.

For what concerns materials of type III and IV, Fig. 5 shows that the predictions of incompressible and compressible models are very different. These materials are compressible even in the range of small strains. Accordingly, both pressure vs. deflection and pressure vs. volume curves start to deviate at low values of $\bar{\delta}$ and $\bar{V}$. Relative differences up to 13% are observed in the maximum pressure and 44% in the deflection. It goes without saying that for these materials the assumption of incompressibility is totally unacceptable.

We remark that the above comparison was presented to show the effect of compressibility in bidimensional problems, starting from the same response in simple tension. In conclusion, the most interesting results are observed for type II materials. Even if in simple tension they exhibit volume changes only for large deformations, in the membrane problem significant differences between compressible and incompressible models arise in the range of moderate deformations. Moreover, this range coincides with the limit pressure point (when present), leading to

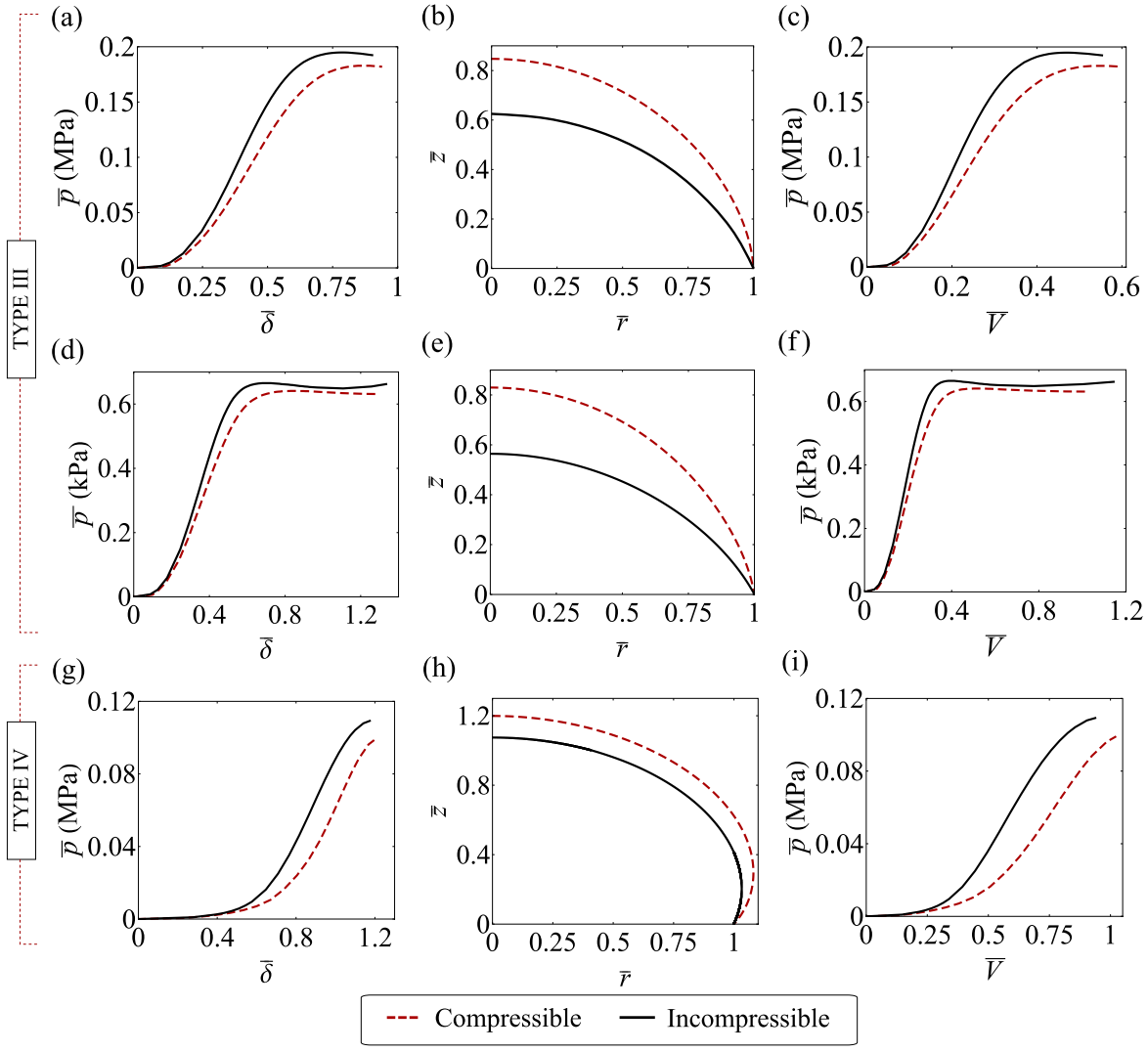

Fig. 5. Inflation of a circular flat membrane. The results are shown for (a)–(c) foam, (d)–(f) hydrogel, (g)–(i) auxetic foam, in terms of normalized pressure $\bar{p} = pL/H$ vs. deflection $\bar{\delta} = \delta/L$ curve, normalized deformed shapes ($\bar{r} = r/L$, $\bar{z} = z/L$) and normalized pressure $\bar{p} = pL/H$ vs. volume $\bar{V} = V/(\pi L^3)$ curve. For each material, the deformed shape corresponds to the value of maximum pressure on the compressible curves.

important consequences in practical applications. Note that, except for type I materials which show almost identical responses, the inflating pressure for compressible models is always lower than the inflating pressure for incompressible models.

5.2. Infinite thin-walled cylindrical tube

The results of the inflation of infinite thin-walled cylindrical tubes are obtained by solving Eq. (18) for each material type, and are displayed in Fig. 6 in terms of pressure vs. deflection curves. Since the solution is uniform (the tube expands laterally homogeneously), the deformed shape is completely described by parameter $\lambda_{2,\infty}$ and the only difference between incompressible and compressible models is in the inflating pressure.

Regarding type I materials, a discrepancy between the compressible and incompressible models appears only for large deformations, when the materials start to show small volume changes (see Fig. 1(d)). In particular, Fig. 6(a) shows that the incompressible model for NR rubber overestimates the final pressure by 7%. Hence, even for a material that is nearly incompressible for any magnitude of deformation, a non-negligible discrepancy between the two models is found. For materials of type II, III and IV the differences increase and occur for moderate deformations. Again, when the material exhibits a limit pressure point, the error between compressible and incompressible models concentrates in that area.

As the inflation increases, the tube reaches a critical stretch $\lambda_{2,c}$ that triggers the bifurcated state and the appearance of a bulge. This point is crucial for practical applications and is determined by Eq. (19). As Fu et al. [41] showed for incompressible materials, if $\left(\partial^2 W/\partial\lambda_1^2\right)^{(\infty)} > 0$ the bifurcation can take place only when the inflating pressure is increasing. Since the sign of $\left(\partial^2 W/\partial\lambda_1^2\right)^{(\infty)}$ does not depend on the volumetric part of the SED, this holds also for compressible materials. Therefore, bifurcation takes place before the limit pressure regardless of material compressibility. The critical stretches computed by Eq. (19) for both compressible and incompressible models are shown in Table 1, along with the stretches corresponding to the limit pressure. Note that when the material exhibits a limit pressure (EPDM, foam, gel and auxetic foam), the critical stretch of the compressible model is always greater than the critical stretch of the incompressible one. On the contrary, when the material response is monotonic, the opposite happens. Ultimately, in case of compressibility the bifurcation points slightly vary quantitatively but they do not differ qualitatively from the incompressible case.

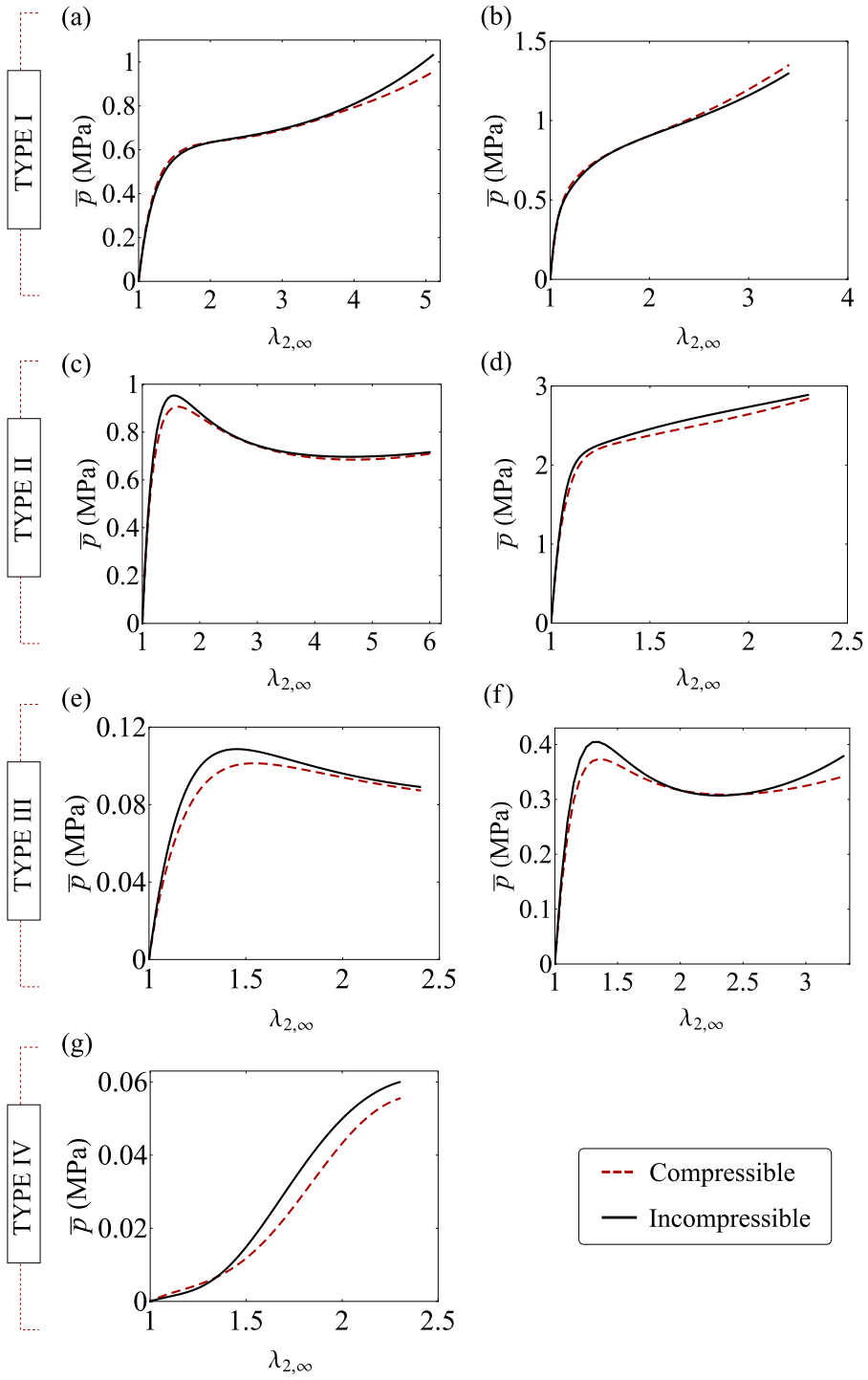

Fig. 6. Uniform inflation of an infinite thin-walled cylindrical tube. The results are shown for (a) NR, (b) silicone, (c) EPDM, (d) NBR, (e) foam, (f) hydrogel and (g) auxetic foam. The curves are represented in terms of normalized pressure $\bar{p} = pL/H$ vs. uniform stretch $\lambda_{2,\infty} = r_\infty/L$.

Table 1
Inflation of thin-walled cylindrical tubes: values of stretch at bifurcation $\lambda_{2,c}$ and stretch at limit pressure $\lambda_{2,p_{max}}$. When $\lambda_{2,c}$ is reached, the uniform solution shifts to the bifurcated state. The values are reported for all the materials considered, for both compressible and incompressible models.

		Type I		Type II		Type III		Type IV
		NR	Silicone	EPDM	NBR	Foam	Hydrogel	Auxetic foam
Compressible	$\lambda_{2,c}$	1.60	1.68	1.48	1.45	1.46	1.33	2.33
	$\lambda_{2,p_{max}}$	/	/	1.61	/	1.54	1.36	2.41
Incompressible	$\lambda_{2,c}$	1.63	1.70	1.45	1.52	1.39	1.30	2.15
	$\lambda_{2,p_{max}}$	/	/	1.55	/	1.45	1.32	2.45

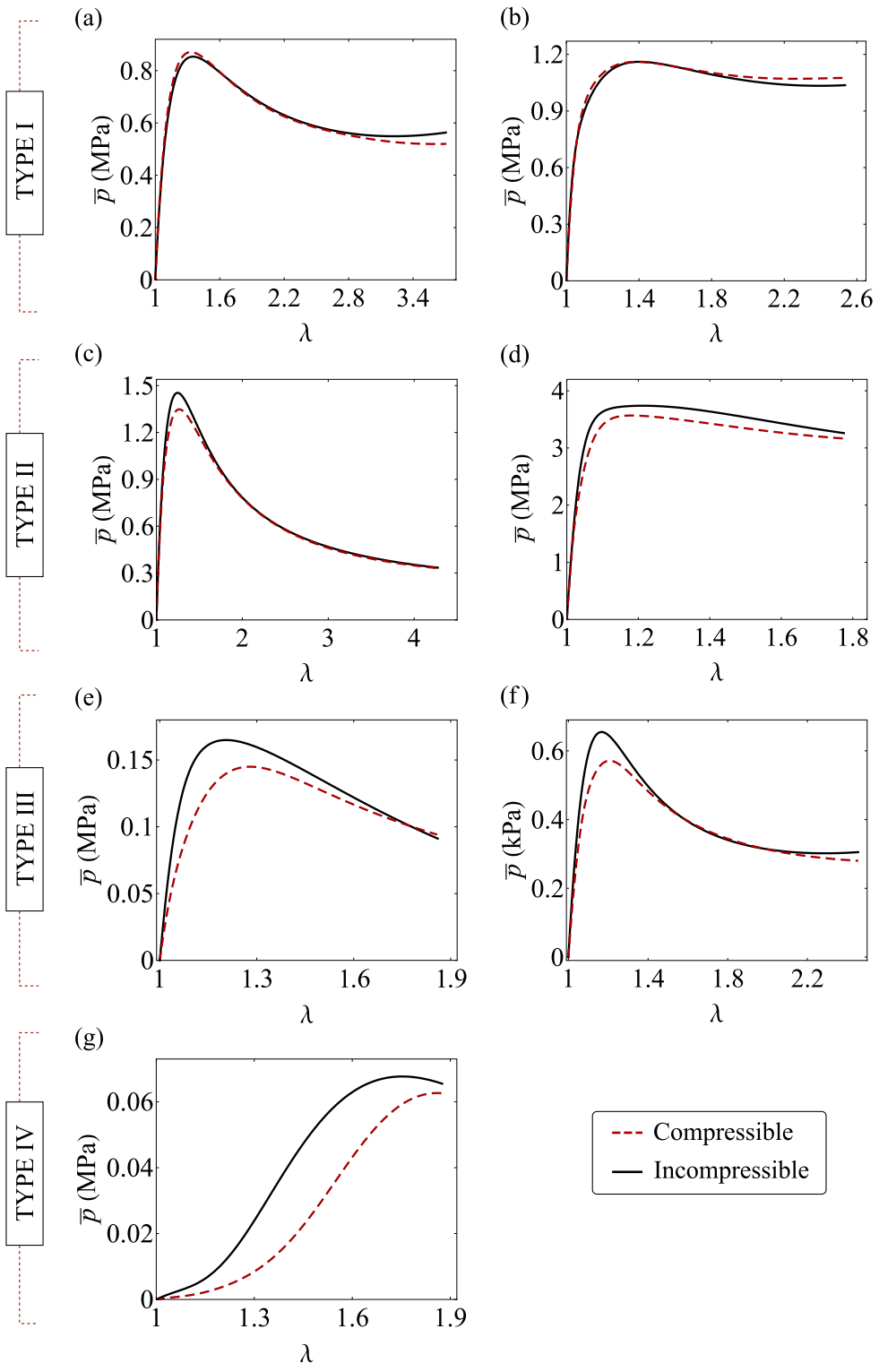

Fig. 7. Inflation of a thin-walled spherical balloon. The results are shown for (a) NR, (b) silicone, (c) EPDM, (d) NBR, (e) foam, (f) hydrogel and (g) auxetic foam. The curves are represented in terms of normalized pressure $\bar{p} = pL/H$ vs. stretch $\lambda = r/L$.

5.3. Thin-walled spherical balloon

The results of the inflation of a spherical balloon are obtained by solving Eqs. (22) and (D.9) for compressible and incompressible models respectively, and are displayed in Fig. 7. Comparing the pressure vs. deflection curves from the three equilibrium problems (Figs. 4, 5, 6 and 7), we notice that the spherical balloon exhibits the greatest discrepancies between the incompressible and compressible models. This is particularly evident for materials of type III and IV, for which the compressibility is more pronounced. Differences up to 18% in the maximum value of internal pressure are observed (see Fig. 7(f)).

The above results may be explained by considering the different strain and stress states in each problem. In the inflation of a spherical balloon, the principal stretches λ_1 and λ_2 are equal to each other

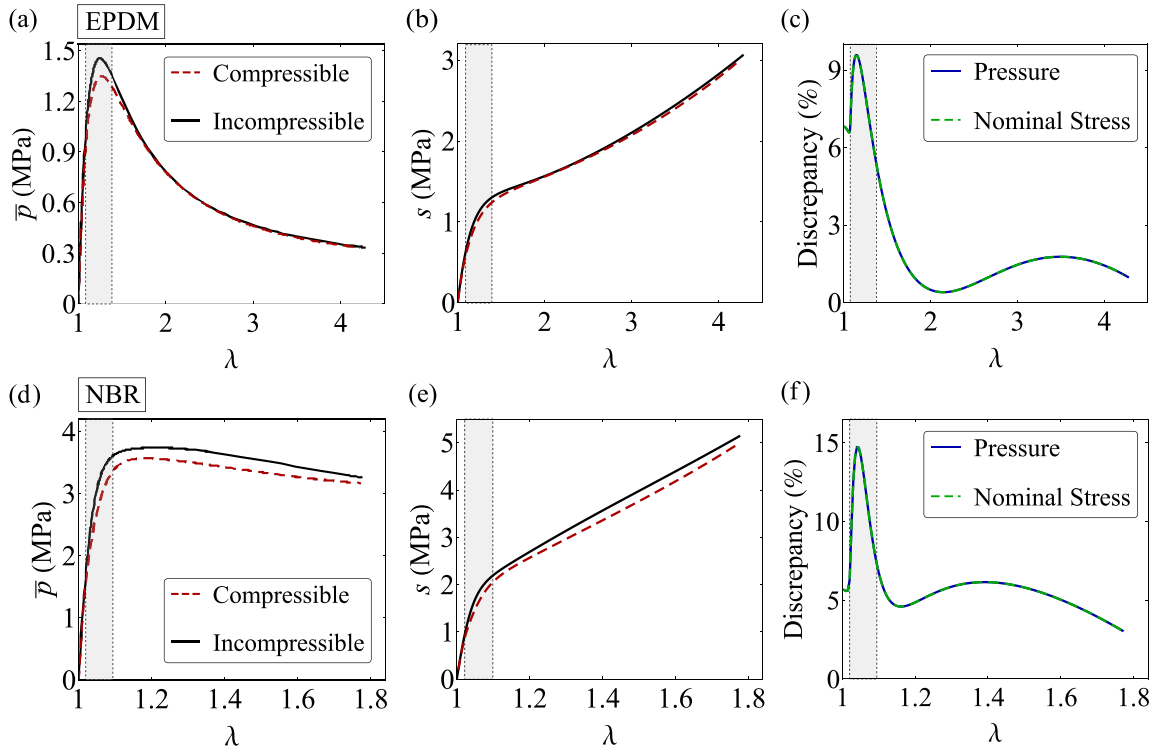

Fig. 8. Comparison between EPDM and NBR inflated spherical balloons. Figs. (a), (b) and (c) respectively show pressure vs. stretch, nominal stress vs. stretch and relative discrepancy in pressure and stress curves between compressible and incompressible models for EPDM. Figs. (d), (e) and (f) depict the corresponding curves for NBR. For a spherical balloon, the stress state is equibiaxial and therefore the discrepancy in pressure curves and nominal stress curves coincides. Major discrepancies are observed near the limit point region in the pressure vs. stretch curves, which corresponds to the transition region between linear and nonlinear behavior in the stress vs. stretch curves.

and the body is under equibiaxial tension. Among the three problems considered, this stress state differs the most from the one in simple tension, where the parameters of both compressible and incompressible models were calibrated to obtain the same response. Thus, it seems reasonable that in this problem compressible and incompressible models show the greatest differences. On the other hand, in the uniform inflation of a cylindrical tube, λ_2 increases whereas λ_1 remains always equal to 1. The principal stress T_1 is much smaller than T_2 and this condition is relatively similar to the stress state in simple tension. For this reason, since their parameters were calibrated to obtain the same uniaxial response, the compressible and incompressible solutions are more similar compared to the case of inflated balloons. Finally, the inflation of a circular flat membrane is an intermediate case. At the pole the stress state is equibiaxial with $\lambda_1 = \lambda_2$ and $T_1 = T_2$, but at the outer boundary $\lambda_2 = 1$ and the stress state is closer to the one in simple tension. In fact, the differences between compressible and incompressible models appear greater than those of the cylindrical tube, but lower than those of the spherical balloon.

In conclusion, the results obtained showed that compressibility plays an important role in the overall response of membrane structures subjected to inflation. We remark that the results in terms of transversal stretch were not presented because, from a practical point of view, it is of no interest in bidimensional problems. Obviously, major differences would be observed in materials of types III and IV, while material types I and II would exhibit relatively lower ones (as can be deduced from Figs. 1(d)–(f)).

5.4. Further considerations

In light of the results shown above, some further considerations on the effect of compressibility in inflated membranes can be drawn. As a general observation, a common trend of maximum discrepancy between compressible and incompressible models is observed around the limit point region. To provide an insight into this behavior, it is convenient to consider the inflation of a spherical balloon, where the principal stretches λ_1 and λ_2 are equal at every point, resulting in an equibiaxial stress state. Fig. 8 shows the pressure vs. stretch, nominal stress vs. stretch and relative discrepancy between compressible and incompressible models in the pressure and stress curves of EPDM and NBR. As indicated by Figs. 8(c) and 8(f), the discrepancies between the two models in the pressure and stress curves are identical. In fact, considering Eq. (21) with $\sigma = s/(\lambda\lambda_3)$, $h = \lambda_3 H$ and $r = \lambda L$, the relation between the nominal stress and the pressure is

$$s = \frac{\lambda^2 L}{2H} p, \tag{24}$$

namely the pressure and the nominal stress are proportional by a factor independent of compressibility. The limit point region in the pressure curves aligns with the transition region between linear and nonlinear behavior in the stress vs. stretch curves. This specific region exhibits the major discrepancy between stress computed from compressible and incompressible models, thereby leading to a more pronounced discrepancy in the pressure curves. The marked discrepancy in nominal stress between compressible and incompressible models observed in this region can be explained by the high rate of change in stiffness specific to this area.

The inflation of cylindrical tubes and the inflation of circular membranes are increasingly complex problems. In particular, in the latter case the stresses vary at each point radially along the membrane. Discrepancies in the nominal stress between compressible and incompressible models are still primarily responsible for discrepancies in the pressure curves, but further phenomena like limit point instability now play an important role in the membrane response. Fig. 9 compares the response of EPDM and NBR rubbers in the case of a circular membrane, showing the deformed shapes and the volume change along the radius for increasing values of deformation. In the case of EPDM, the pressure

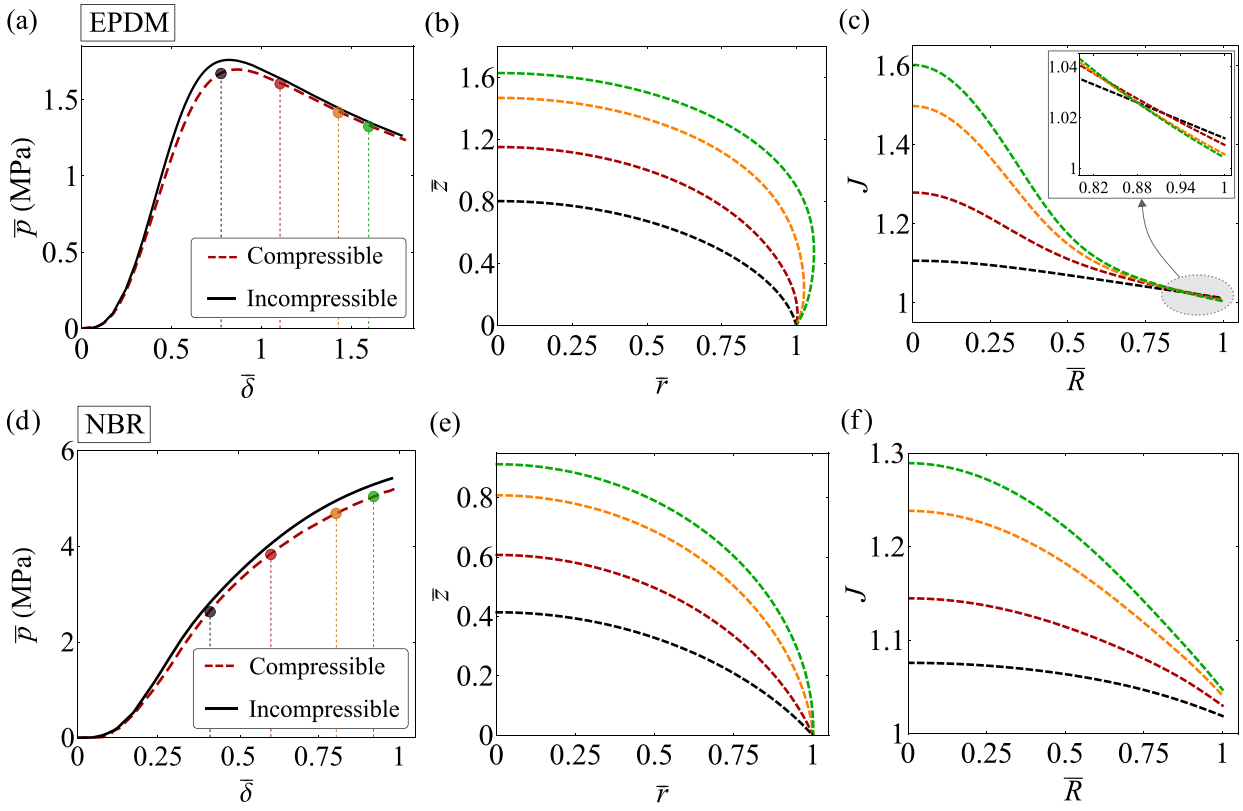

Fig. 9. Comparison between EPDM and NBR inflated circular membranes. Figs. (a), (b) and (c) respectively show pressure vs. deflection curves, deformed shapes and volume changes in the domain for EPDM, while Figs. (d), (e) and (f) depict the corresponding curves for NBR. In the case of EPDM, the $\bar{p}$ vs. $\bar{\delta}$ curve exhibits a limit point that triggers an unstable softening branch. Correspondingly, the deformed shape shows lateral expansion, and the volume change starts to decrease at the outer boundary of the domain. In the case of NBR, the $\bar{p}$ vs. $\bar{\delta}$ curve is monotonic, and the change in volume increases with deformation throughout the domain.

curve exhibits a limit point, where the discrepancy between compressible and incompressible models is maximum, followed by a softening branch, where the two models converge to the same curve. The limit point triggers an instability characterized by a lateral expansion, as indicated in Fig. 9(b). Fig. 9(c) shows how, after the limit point, the change in volume starts to decrease at the outer boundary. Therefore, as the deformation increases, in the outer region compressibility has less effect since the change in volume reduces. On the contrary, in the case of NBR the limit point is not reached. The pressure is monotonic and the volume change continues to increase in the entire domain of the membrane (see Fig. 9(f)). Accordingly, the relative discrepancy between compressible and incompressible models slightly increases as the deformation increases. In conclusion, when limit point instability occurs, the effect of compressibility tends to reduce along the unstable softening branch.

6. Conclusions

Existing models for highly deformable membranes primarily focus on incompressible or nearly compressible materials. In the present work, we investigated the effect of material compressibility on the mechanics of inflated membranes. We proposed a novel numerical solution for the inflation of circular membranes and extended well-established elastic solutions for thin-walled cylindrical tubes and spherical balloons. We considered experimental data of compressible elastomers, polymeric foams, and hydrogels. To the best of our knowledge, this is the first comprehensive analysis of membrane problems considering real behaviors of materials with large volumetric deformations.

The results showed that compressibility may sensibly affect the response of inflated membranes. Despite these problems being addressed under the assumption of two-dimensional solid, volumetric deformations play a significant role. It is demonstrated that incompressible models are generally unsuitable and may lead to significant errors in predicting limit pressure and deformed shape. Therefore, the presented numerical solutions establish benchmarks for advancing the modeling and utilization of foam and hydrogel membranes in engineering technologies. Additionally, the applicability of the proposed models extends beyond conventional materials, including highly stretchable membrane-type metamaterials [80–83]. As a future step, we aim to strengthen the findings of this work through an experimental investigation on polymeric foams and hydrogel membranes.

CRediT authorship contribution statement

Stefano Sirotti: Writing – review & editing, Writing – original draft, Methodology, Investigation, Data curation, Conceptualization. **Matteo Pelliciari:** Writing – review & editing, Writing – original draft, Methodology, Investigation, Conceptualization. **Angelo Marcello Tarantino:** Funding acquisition.

Declaration of competing interest

The authors declare that they have no known competing financial interests or personal relationships that could have appeared to influence the work reported in this paper.

Data availability

Data will be made available on request.

Acknowledgments

This work was supported by the Italian Ministry of University and Research (MUR) through research grant PRIN 2022 PNRR No. P2022AHFCP on "New challenges of thin-walled structures at large strains and their promising applications" and PRIN 2022 PNRR No. P2022ATTAR on "Energy harvesting via naturally induced piezoelectric vibration with a view towards application". Financial support from the University of Modena and Reggio Emilia in the framework of "FAR Dipartimentale 2023-2024" (CUP E93C23000280005) is gratefully acknowledged. Support by the National Group of Mathematical Physics (GNFM-INdAM) is also acknowledged.

Appendix A. Equilibrium solution in simple tension

The compressible isotropic material is defined by a stored energy function $W(I_1, I_2, I_3)$. We set the reference system x, y, z, with x being the longitudinal axis of the solid. The nominal stresses are indicated by s_i and the true stresses by σ_i, with $i = x, y, z$. The lateral stresses s_y and s_z are both identically zero. The lateral stretches λ_y and λ_z are equal to each other.

The equilibrium solution in simple tension reads [84]

$$w_1 + \left(\lambda_x^2 + \lambda_y^2\right) w_2 + \lambda_x^2 \lambda_y^2 w_3 = 0, \tag{A.1}$$

$$s_x = 2\lambda_x \left(w_1 + 2\lambda_y^2 w_2 + \lambda_y^4 w_3\right), \tag{A.2}$$

where $w_j = \partial W / \partial I_j$, with $j = 1, 2, 3$. For each value of longitudinal stretch λ_x, the lateral stretch λ_y is computed by solving Eq. (A.1), which is in general an implicit equation. Then, the nominal stress s_x is computed from Eq. (A.2) and the true stress by $\sigma_x = s_x / \lambda_y^2$.

In the case of incompressible model we have that $J = 1$, from which it follows that $\lambda_y = 1/\sqrt{\lambda_x}$. The equilibrium equation reduces to

$$s_x = 2\left(1 - \frac{1}{\lambda_x^3}\right)\left(\lambda_x w_1 + w_2\right). \tag{A.3}$$

Appendix B. Optimal values of model parameters

Tables B.2 and B.3 present the parameters obtained from the fitting described in Section 3.2.

Appendix C. Finite element simulations

The FE simulations on circular inflated membranes were carried out in software COMSOL Multiphysics version 6.0. The model was created using the 3D membrane interface and a stationary study was carried out. The circular membrane was generated by defining a circle in a work plane. The diameter of the circle was set to 30 mm and the thickness to 1 mm. The edges of the membrane were fixed. The flat membrane in the undeformed configuration had no transverse stiffness. Thus, a small tensile prestress was necessarily applied by introducing an external in-plane force of 0.1 N/m. Note that this prestress was negligible compared to the stress values arising during the simulation.

The membrane was discretized in a fine mesh, as shown in Fig. C.10(a). The deviatoric invariant $\bar{I}_1$ was introduced as variable and the compressible hyperelastic material model was defined. In particular, the combined SED is $W\left(\bar{I}_1, J\right) = W_d\left(\bar{I}_1\right) + W_h(J)$, where the deviatoric and volumetric contributions are expressed respectively by Eqs. (4) and (6). The expression of the SED was written in the user-defined hyperelastic material. The membrane was subjected to inflation by applying a pressure load that increased linearly in a quasi-static manner. Fig. C.10(b) shows the deformed configuration of the circular inflated membrane.

The sole purpose of the FE simulations was to validate the numerical solution proposed in Section 4.1. Hence, for the sake of clarity, we present the results only for one material for each of the four types. In particular, the following materials were considered: silicone, EPDM, foam by [70] and auxetic foam by [72]. The results of the simulations are presented in Fig. C.11 and show that the proposed numerical solution matches well the FE result.

Appendix D. Equilibrium solutions for incompressible membranes under inflation

In the following, we derive the solution of each membrane problem studied in this work considering an incompressible material. Under the assumption of material incompressibility every deformation is isochoric, namely the material cannot experience volume changes. The strain energy function is dependent on I_1 and I_2 only, $W = W\left(I_1, I_2\right)$, and the principal Cauchy stresses are given by

$$\sigma_i = \lambda_i \frac{\partial W}{\partial \lambda_i} - P, \quad i = 1, 2, 3 \text{ (no summation)}, \tag{D.1}$$

where P is the internal pressure due to the incompressibility constraint. The transversal stretch λ_3 is related to the principal stretches by $\lambda_3 =$

Table B.2
Optimal parameters of the incompressible Yeoh–Fleming model for the materials considered in this work. The fitting was performed on the stress vs. stretch data in simple tension. If applicable, the units are in MPa.

	NR	Silicone	EPDM	NBR	Foam	Hydrogel	Auxetic foam
A	0.27	0.43	0.29	1.28	0.033	0.89×10^{-4}	−0.147
B	0.078	1.72×10^{-3}	7×10^{-3}	2.16×10^{-3}	0.001	0.0377	−1.026
C_{10}	0.09	0.49	0.44	2.74	0.06	0.34×10^{-3}	0.149
I_m	0.02	2.96	1.49	2.94	2.13	2.48	1.32

Table B.3
Optimal parameters of the compressible SED proposed in [35] for the materials considered in this work. The fitting procedure is described in Section 3.2. The last line shows the values of the corresponding Poisson ratio ν, computed by Eq. (7). If applicable, the units are in MPa.

	NR	Silicone	EPDM	NBR	Foam	Hydrogel	Auxetic foam
A	0.258	0.417	0.313	1.31	0.0516	1.37×10^{-4}	−0.258
B	0.074	4.32×10^{-3}	0.03	7.82×10^{-3}	0.0101	0.0187	−1.088
C_{10}	0.121	0.397	0.373	2.59	0.065	3.73×10^{-4}	0.27
I_m	0.628	2.92	1.3	2.93	2.50	2.714	2.45
κ	710	670	490	410	0.5956	0.0027	0.0019
β_1	7.09	5.03	2.23	4.18	2.34	7.08	4.58
β_2	69.25	68.86	9.05	14.03	31.7	17.22	2.18
β_3	13.14×10^{-4}	1×10^{-4}	6.88×10^{-4}	13.76×10^{-4}	0.321	0.0764	0.0954
q	0.723	0.461	0.974	0.953	0.327	0.751	0.65
ν	0.499	0.499	0.498	0.491	0.326	0.332	−0.712

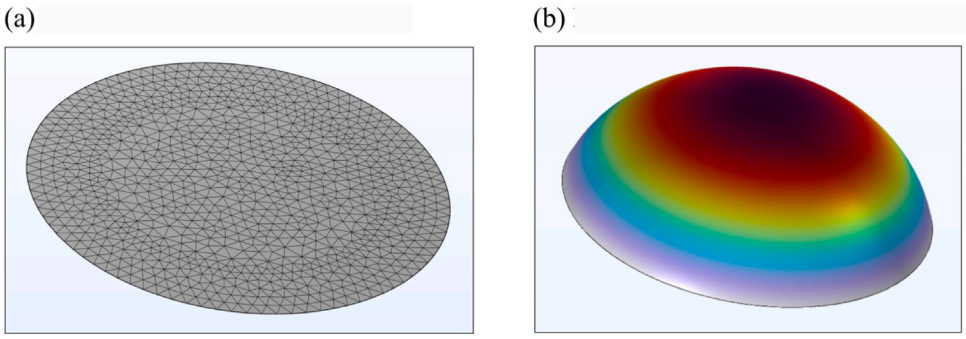

Fig. C.10. FE model of the circular inflated membrane in COMSOL. (a) Membrane mesh in the undeformed configuration. (b) Deformed membrane after the application of the pressure load. The compressible SED, $W\left(\bar{I}_1, J\right) = W_d\left(\bar{I}_1\right) + W_h(J)$, was introduced as a user-defined hyperelastic material.

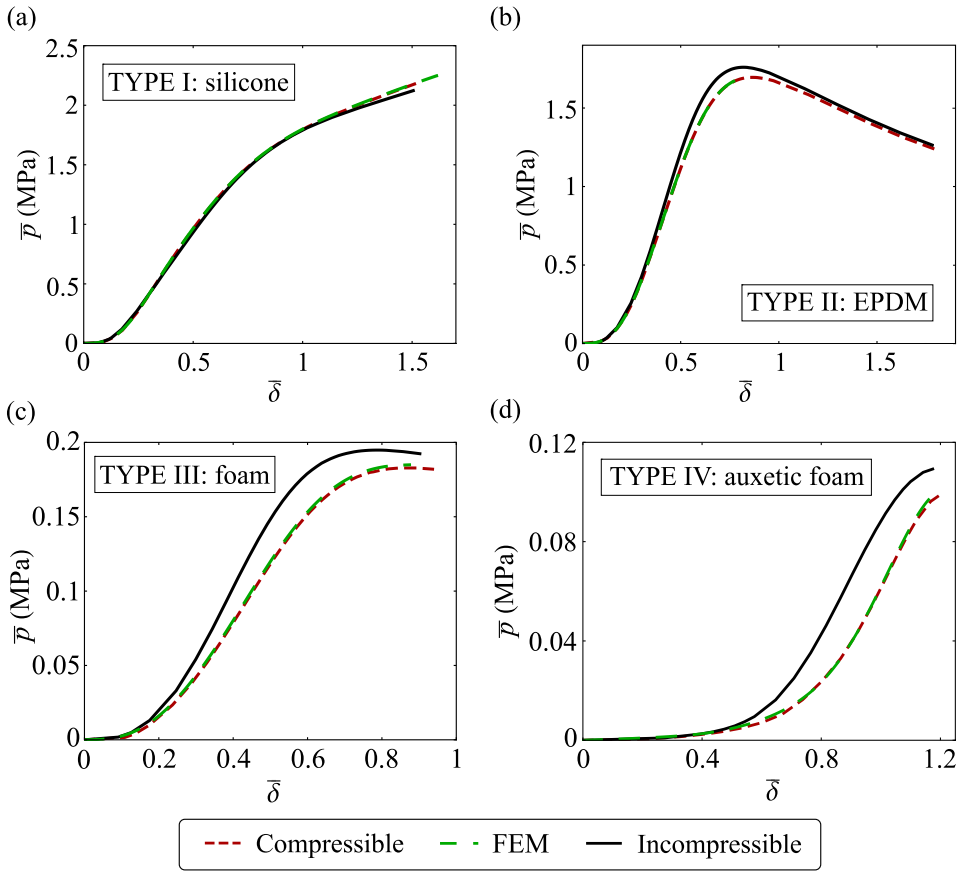

Fig. C.11. FE validation of the proposed solution for the inflation of circular compressible membranes. The results are shown for (a) silicone, (b) EPDM, (c) foam and (d) auxetic foam. The curves are represented in terms of normalized pressure $\bar{p} = pL/H$ vs. displacement $\bar{\delta} = \delta/L$.

$1/\left(\lambda_1\lambda_2\right)$. Using this relation and the membrane assumption $\sigma_3 = 0$, the internal pressure P is determined and the principal Cauchy stresses reduce to

$$\sigma_i = 2\left(w_1 + \lambda_j^2 w_2\right)\left(\lambda_i^2 - \frac{1}{\lambda_i^2\lambda_j^2}\right), \quad i,j = 1,2. \tag{D.2}$$

We remark that the incompressible Yeoh–Fleming model is given by

$$W\left(I_1\right) = \frac{A}{B}\left(I_m - 3\right)\left(1 - e^{-B(I_1-3)/(I_m-3)}\right) - C_{10}\left(I_m - 3\right)\ln\left(1 - \frac{I_1 - 3}{I_m - 3}\right), \tag{D.3}$$

and the derivatives with respect to I_1 and I_2 are

$$w_1 = Ae^{-\frac{B\left(I_1-3\right)}{I_m-3}} + \frac{C_{10}}{1 - \frac{I_1-3}{I_m-3}}, \quad w_2 = 0. \tag{D.4}$$

D.1. Circular flat membrane

The principal stress resultants T_1 and T_2 read

$$T_i = 2H\left(w_1 + \lambda_j^2 w_2\right)\left(\frac{\lambda_i}{\lambda_j} - \frac{1}{\lambda_i^3\lambda_j^3}\right), \quad i,j = 1,2. \tag{D.5}$$

Substituting these relations into the equilibrium equations, Eq. (11), the following governing system of differential equations is obtained:

$$\begin{aligned}
\lambda_1' &= \frac{w_1\psi_1 + w_2\psi_2 + \frac{\partial w_1}{\partial \lambda_2}\psi_3 + \frac{\partial w_2}{\partial \lambda_2}\psi_4}{R\lambda_2\left(3w_1 - \frac{\partial w_1}{\partial \lambda_1}\lambda_1 + \left(3w_2 - \frac{\partial w_2}{\partial \lambda_1}\lambda_1 + \lambda_1^4\left(w_1 + \frac{\partial w_1}{\partial \lambda_1}\lambda_1\right)\right)\lambda_2^2 + \lambda_1^4\left(w_2 + \frac{\partial w_2}{\partial \lambda_1}\lambda_1\right)\lambda_2^4\right)}, \\
\lambda_2' &= \frac{\eta - \lambda_2}{R}, \\
\eta' &= \frac{\eta\lambda_1'}{\lambda_1} - \frac{\phi\lambda_1^5\lambda_2^4\sqrt{-\eta^2 + \lambda_1^2} + 2\lambda_1\left(\eta^2 - \lambda_1^2\right)\left(w_1 + w_2\lambda_1^2\right)\left(\lambda_1^2\lambda_2^4 - 1\right)}{2R\lambda_1\lambda_2\left(w_1 + w_2\lambda_2^2\right)\left(\lambda_1^4\lambda_2^2 - 1\right)},
\end{aligned} \tag{D.6}$$

where $\phi = pR/H$ and, for the sake of clarity, the following quantities were defined:

$$\begin{aligned}
\psi_1 &= \eta\lambda_2^4\lambda_1^3 - 3\eta\lambda_1 - \lambda_2^3\lambda_1^5 + 3\lambda_2\lambda_1, \\
\psi_2 &= -\eta\lambda_2^4\lambda_1^5 - \eta\lambda_1^3 + \lambda_2^5\lambda_1^5 + \lambda_2^3\lambda_1, \\
\psi_3 &= -\eta\lambda_2^3\lambda_1^5 + \eta\lambda_2\lambda_1 + \lambda_2^4\lambda_1^5 - \lambda_2^2\lambda_1, \\
\psi_4 &= -\eta\lambda_1^5\lambda_2^5 + \eta\lambda_1\lambda_2^3 + \lambda_1^5\lambda_2^6 - \lambda_1\lambda_2^4.
\end{aligned} \tag{D.7}$$

In this case the integration is more straightforward than the compressible model because the transversal stretch is simply determined by the incompressibility constraint. Thus, it does not need to be computed numerically at each step. Ultimately, the integration reduces to the following steps: (i) set an initial condition λ_0 at the pole and a guess value p_0 for the pressure; (ii) integrate system (D.6) for increasing values of R, until $\lambda_2 = 1$. The value of R corresponding to $\lambda_2 = 1$ is denoted by R^*; (iii) scale the guess value p_0 by the factor $\gamma = L/R^*$ to obtain the correct pressure, $p_1 = p_0/\gamma = p_0 R^*/L$; (iv) integrate again system (D.6) with the correct pressure to obtain the stretches profiles; (v) repeat the procedure for different initial conditions λ_0 to build the pressure curve.

D.2. Infinite thin-walled cylindrical tube

In the case of an incompressible material, the pressure curve relative to uniform inflation is written as

$$\bar{p} = \frac{2\left(\lambda_{2,\infty}^4 - 1\right)\left(w_1^{(\infty)} + w_2^{(\infty)}\right)}{\lambda_{2,\infty}^4}, \tag{D.8}$$

where $\bar{p} = pL/H$ is the normalized pressure, $w_1^{(\infty)}$ and $w_2^{(\infty)}$ are the derivatives of W with respect to I_1 and I_2 evaluated at $\lambda_1 = 1$ and $\lambda_2 = \lambda_{2,\infty} = r_\infty/L$.

The bifurcation condition maintains the formal expression of Eq. (19). We remark that since the transversal stretch λ_3 is given by $1/\left(\lambda_1\lambda_2\right)$, the computation of $\partial^2 W/\partial\lambda_1^2$, $\partial W/\partial\lambda_2$, $\partial^2 W/\partial\lambda_2^2$ and $\partial^2 W/\partial\lambda_1\partial\lambda_2$ is straightforward.

D.3. Thin-walled spherical balloon

In this case the principal stretches are equal, $\lambda_1 = \lambda_2 = \lambda$, therefore $\lambda_3 = 1/\lambda^2$. The equilibrium equation reduces to the explicit relation

$$\bar{p} = 4\left(\lambda^{-1} - \lambda^{-7}\right)\left(w_1 + \lambda^2 w_2\right), \tag{D.9}$$

with $\bar{p} = pL/H$.

References

[1] Stewart BG, Sitaraman SK. Biaxial inflation stretch test for flexible electronics. Adv Energy Mater 2021;2001503.

[2] Liu Z, McBride A, Sharma BL, Steinmann P, Saxena P. Coupled electro-elastic deformation and instabilities of a toroidal membrane. J Mech Phys Solids 2021;151:104221.

[3] Gorissen B, Milana E, Baeyens A, Broeders E, Christiaens J, Collin K, et al. Hardware sequencing of inflatable nonlinear actuators for autonomous soft robots. Adv Mater 2019;31(3):1804598.

[4] Chen L, Chen W, Xue Y, Zhang M, Chen X, Cao X, et al. Investigation of the state transition and moving boundary in a pneumatic–hydraulic coupled dielectric elastomer actuator. J Appl Mech 2019;86(3):031004.

[5] Walker J, Zidek T, Harbel C, Yoon S, Strickland FS, Kumar S, et al. Soft robotics: A review of recent developments of pneumatic soft actuators. In: Actuators, vol. 9, (no. 1):Multidisciplinary Digital Publishing Institute; 2020, p. 3.

[6] Goulbourne N, Mockensturm E, Frecker M. A nonlinear model for dielectric elastomer membranes. J Appl Mech 2005;72(6):899–906.

[7] Fox JW, Goulbourne NC. On the dynamic electromechanical loading of dielectric elastomer membranes. J Mech Phys Solids 2008;56(8):2669–86.

[8] Grosjean C, Lee GB, Hong W, Tai YC, Ho CM. Micro balloon actuators for aerodynamic control. In: Proceedings MEMS 98. iEEE. Eleventh annual international workshop on micro electro mechanical systems. An investigation of micro structures, sensors, actuators, machines and systems. cat. no. 98CH36176. IEEE; 1998, p. 166–71.

[9] Vandeparre H, Watson D, Lacour SP. Extremely robust and conformable capacitive pressure sensors based on flexible polyurethane foams and stretchable metallization. Appl Phys Lett 2013;103(20):204103.

[10] Doutres O, Atalla N, Dong K. Effect of the microstructure closed pore content on the acoustic behavior of polyurethane foams. J Appl Phys 2011;110(6):064901.

[11] Hailan SM, Ponnamma D, Krupa I. The separation of oil/water mixtures by modified melamine and polyurethane foams: A review. Polymers 2021;13(23):4142.

[12] Yang HC, Gong JL, Zeng GM, Zhang P, Zhang J, Liu HY, et al. Polyurethane foam membranes filled with humic acid-chitosan crosslinked gels for selective and simultaneous removal of dyes. J Colloid Interface Sci 2017;505:67–78.

[13] Yazdi MK, Vatanpour V, Taghizadeh A, Taghizadeh M, Ganjali MR, Munir MT, et al. Hydrogel membranes: A review. Mater Sci Eng: C 2020;114:111023.

[14] Serina ER, Mockensturm E, Mote Jr CD, Rempel D. A structural model of the forced compression of the fingertip pulp. J Biomech 1998;31(7):639–46.

[15] Murphy JG, Rajagopal KR. Inflation of residually stressed fung-type membrane models of arteries. J Mech Behav Biomed Mater 2021;122:104699.

[16] Takashima K, Kitou T, Mori K, Ikeuchi K. Simulation and experimental observation of contact conditions between stents and artery models. Med Eng Phys 2007;29(3):326–35.

[17] Buerzle W, Haller CM, Jabareen M, Egger J, Mallik AS, Ochsenbein-Koelble N, et al. Multiaxial mechanical behavior of human fetal membranes and its relationship to microstructure. Biomech Model Mechanobiol 2013;12:747–62.

[18] Hong W, Zhao X, Zhou J, Suo Z. A theory of coupled diffusion and large deformation in polymeric gels. J Mech Phys Solids 2008;56(5):1779–93.

[19] Ding Z, Liu Z, Hu J, Swaddiwudhipong S, Yang Z. Inhomogeneous large deformation study of temperature-sensitive hydrogel. Int J Solids Struct 2013;50(16–17):2610–9.

[20] Ahearne M, Yang Y, El Haj AJ, Then KY, Liu KK. Characterizing the viscoelastic properties of thin hydrogel-based constructs for tissue engineering applications. J R Soc Interface 2005;2(5):455–63.

[21] Liu Z, Hong W, Suo Z, Swaddiwudhipong S, Zhang Y. Modeling and simulation of buckling of polymeric membrane thin film gel. Comput Mater Sci 2010;49(1):S60–4.

[22] Rampf M, Speck O, Speck T, Luchsinger RH. Self-repairing membranes for inflatable structures inspired by a rapid wound sealing process of climbing plants. J Bion Eng 2011;8(3):242–50.

[23] Pientka Z, Pokorný P, Belafi-Bako K. Closed-cell polymeric foam for hydrogen separation and storage. J Membr Sci 2007;304(1–2):82–7.

[24] Elele E, Shen Y, Tang J, Lei Q, Khusid B, Tkacik G, et al. Mechanical properties of polymeric microfiltration membranes. J Membr Sci 2019;591:117351.

[25] Landauer AK, Li X, Franck C, Henann DL. Experimental characterization and hyperelastic constitutive modeling of open-cell elastomeric foams. J Mech Phys Solids 2019;133:103701.

[26] Nafo W, Al-Mayah A. Measuring hyperelastic properties of hydrogels using cavity expansion method. Exp Mech 2019;59(7):1047–61.

[27] Sasson A, Patchornik S, Eliasy R, Robinson D, Haj-Ali R. Hyperelastic mechanical behavior of Chitosan hydrogels for nucleus pulposus replacement–experimental testing and constitutive modeling. J Mech Behav Biomed Mater 2012;8:143–53.

[28] Ogden RW, Saccomandi G, Sgura I. Fitting hyperelastic models to experimental data. Comput Mech 2004;34:484–502.

[29] Khajehsaeid H, Arghavani J, Naghdabadi R. A hyperelastic constitutive model for rubber-like materials. Eur J Mech A Solids 2013;38:144–51.

[30] Horgan CO. The remarkable Gent constitutive model for hyperelastic materials. Int J Non-Linear Mech 2015;68:9–16.

[31] Zhang Y, Yu K, Lee KH, Li K, Du H, Wang Q. Mechanics of stretchy elastomer lattices. J Mech Phys Solids 2022;159:104782.

[32] Starkova O, Aniskevich A. Poisson's ratio and the incompressibility relation for various strain measures with the example of a silica-filled SBR rubber in uniaxial tension tests. Polym Test 2010;29(3):310–8.

[33] Kugler HP, Stacer RG, Steimle C. Direct measurement of Poisson's ratio in elastomers. Rubber Chem Technol 1990;63(4):473–87.

[34] Steck D, Qu J, Kordmahale SB, Tscharnuter D, Muliana A, Kameoka J. Mechanical responses of ecoflex silicone rubber: Compressible and incompressible behaviors. J Appl Polym Sci 2019;136(5):47025.

[35] Pelliciari M, Sirotti S, Tarantino AM. A strain energy function for large deformations of compressible elastomers. J Mech Phys Solids 2023;105308.
[36] Treloar LRG. Strains in an inflated rubber sheet, and the mechanism of bursting. Rubber Chem Technol 1944;17(4):957–67.
[37] Adkins JE, Rivlin RS. Large elastic deformations of isotropic materials IX. The deformation of thin shells. Philos Trans R Soc Lond Ser A Math Phys Sci 1952;244(888):505–31.
[38] Yang WH, Feng WW. On axisymmetrical deformations of nonlinear membranes. J Appl Mech 1970;37(4):1002–11.
[39] Patil A, DasGupta A. Finite inflation of an initially stretched hyperelastic circular membrane. Eur J Mech A Solids 2013;41:28–36.
[40] Chaudhuri A, DasGupta A. On the static and dynamic analysis of inflated hyperelastic circular membranes. J Mech Phys Solids 2014;64:302–15.
[41] Fu Y, Pearce S, Liu KK. Post-bifurcation analysis of a thin-walled hyperelastic tube under inflation. Int J Non-Linear Mech 2008;43(8):697–706.
[42] Ye Y, Liu Y, Fu Y. Weakly nonlinear analysis of localized bulging of an inflated hyperelastic tube of arbitrary wall thickness. J Mech Phys Solids 2020;135:103804.
[43] Mao G, Li T, Zou Z, Qu S, Shi M. Prestretch effect on snap-through instability of short-length tubular elastomeric balloons under inflation. Int J Solids Struct 2014;51(11–12):2109–15.
[44] Kyriakides S, Yu-Chung C. On the inflation of a long elastic tube in the presence of axial load. Int J Solids Struct 1990;26(9–10):975–91.
[45] Kyriakides S, Yu-Chung C. The initiation and propagation of a localized instability in an inflated elastic tube. Int J Solids Struct 1991;27(9):1085–111.
[46] Alexander H. Tensile instability of initially spherical balloons. Internat J Engrg Sci 1971;9(1):151–60.
[47] Mangan R, Destrade M. Gent models for the inflation of spherical balloons. Int J Non-Linear Mech 2015;68:52–8.
[48] Kanner LM, Horgan CO. Elastic instabilities for strain-stiffening rubber-like spherical and cylindrical thin shells under inflation. Int J Non-Linear Mech 2007;42(2):204–15.
[49] Liu MX, Wang CG, Li XD. Rigid-flexible contact analysis of an inflated membrane balloon with various contact conditions. Int J Solids Struct 2018;144:218–29.
[50] Patil A, DasGupta A, Eriksson A. Contact mechanics of a circular membrane inflated against a deformable substrate. Int J Solids Struct 2015;67:250–62.
[51] Yang X, Yu L, Long R. Contact mechanics of inflated circular membrane under large deformation: Analytical solutions. Int J Solids Struct 2021;233:111222.
[52] Firouzi N, Żur KK. On the generalized nonlinear mechanics of compressible, incompressible, isotropic, and anisotropic hyperelastic membranes. Int J Solids Struct 2023;264:112088.
[53] Pelliciari M, Sirotti S, Aloisio A, Tarantino AM. Analytical, numerical and experimental study of the finite inflation of circular membranes. Int J Mech Sci 2022;226:107383.
[54] Sirotti S, Pelliciari M, Aloisio A, Tarantino AM. Analytical pressure–deflection curves for the inflation of pre-stretched circular membranes. Eur J Mech A Solids 2023;97:104831.
[55] Chung DT, Horgan CO, Abeyaratne R. The finite deformation of internally pressurized hollow cylinders and spheres for a class of compressible elastic materials. Int J Solids Struct 1986;22(12):1557–70.
[56] Selvadurai APS, Suvorov AP. On the inflation of poro-hyperelastic annuli. J Mech Phys Solids 2017;107:229–52.
[57] Doll S, Schweizerhof K. On the development of volumetric strain energy functions. J Appl Mech 2000;67(1):17–21.
[58] Moerman KM, Fereidoonnezhad B, McGarry JP. Novel hyperelastic models for large volumetric deformations. Int J Solids Struct 2020;193:474–91.
[59] Rivlin RS, Saunders DW. Large elastic deformations of isotropic materials: VII. Experiments on the deformation of rubber. Springer; 1997.
[60] Haines DW, Wilson WD. Strain-energy density function for rubberlike materials. J Mech Phys Solids 1979;27(4):345–60.
[61] Upadhyay K, Subhash G, Spearot D. Thermodynamics-based stability criteria for constitutive equations of isotropic hyperelastic solids. J Mech Phys Solids 2019;124:115–42.
[62] Bischoff JE, Arruda EM, Grosh K. A new constitutive model for the compressibility of elastomers at finite deformations. Rubber Chem Technol 2001;74(4):541–59.
[63] Sansour C. On the physical assumptions underlying the volumetric-isochoric split and the case of anisotropy. Eur J Mech A Solids 2008;27(1):28–39.
[64] Attard MM. Finite strain—isotropic hyperelasticity. Int J Solids Struct 2003;40(17):4353–78.
[65] Steinmann P, Hossain M, Possart G. Hyperelastic models for rubber-like materials: Consistent tangent operators and suitability for Treloar's data. Arch Appl Mech 2012;82:1183–217.
[66] Destrade M, Saccomandi G, Sgura I. Methodical fitting for mathematical models of rubber-like materials. Proc R Soc A: Math Phys Eng Sci 2017;473(2198):20160811.
[67] Mihai LA, Goriely A. How to characterize a nonlinear elastic material? A review on nonlinear constitutive parameters in isotropic finite elasticity. Proc R Soc A: Math Phys Eng Sci 2017;473(2207):20170607.
[68] Dal H, Açıkgöz K, Badienia Y. On the performance of isotropic hyperelastic constitutive models for rubber-like materials: A state of the art review. Appl Mech Rev 2021;73(2).
[69] Yeoh OH, Fleming PD. A new attempt to reconcile the statistical and phenomenological theories of rubber elasticity. J Polym Sci Part B: Polym Phys 1997;35(12):1919–31.
[70] Blatz PJ, Ko WL. Application of finite elastic theory to the deformation of rubbery materials. Trans Soc Rheol 1962;6(1):223–52.
[71] Urayama K, Takigawa T, Masuda T. Poisson's ratio of poly (vinyl alcohol) gels. Macromolecules 1993;26(12):3092–6.
[72] Choi JB, Lakes RS. Non-linear properties of polymer cellular materials with a negative Poisson's ratio. J Mater Sci 1992;27:4678–84.
[73] Liu RC, Jin L, Cai Z, Liu Y. An experimental study of morphological formation in bilayered tubular structures driven by swelling/growth. Math Mech Solids 2022;27(8):1569–91.
[74] Ciarlet PG, Geymonat G. Sur les lois de comportement en élasticité non linéaire compressible. CR Acad. Sci. Paris Sér. II 1982;295:423–6.
[75] Pelliciari M, Tarantino AM. A continuum model for circular graphene membranes under uniform lateral pressure. J Elasticity 2022;151(2):273–303.
[76] Liu Y, Ye Y, Althobaiti A, Xie YX. Prevention of localized bulging in an inflated bilayer tube. Int J Mech Sci 2019;153:359–68.
[77] Haughton D. Elastic membranes. London Math Soc Lecture Note Ser 2001;233–67.
[78] Anssari-Benam A, Bucchi A, Saccomandi G. Modelling the inflation and elastic instabilities of rubber-like spherical and cylindrical shells using a new generalised Neo-Hookean strain energy function. J Elasticity 2022;151(1):15–45.
[79] Haughton D, Ogden R. On the incremental equations in non-linear elasticity – II. bifurcation of pressurized spherical shells. J Mech Phys Solids 1978;26(2):111–38.
[80] Ma F, Wang C, Liu C, Wu JH. Structural designs, principles, and applications of thin-walled membrane and plate-type acoustic/elastic metamaterials. J Appl Phys 2021;129(23).
[81] Chen Y, Huang G, Zhou X, Hu G, Sun CT. Analytical coupled vibroacoustic modeling of membrane-type acoustic metamaterials: Membrane model. J Acoust Soc Am 2014;136(3):969–79.
[82] Bodaghi M, Damanpack A, Hu G, Liao W. Large deformations of soft metamaterials fabricated by 3D printing. Mater Des 2017;131:81–91.
[83] Yan G, Yao S, Li Y. Propagation of elastic waves in metamaterial plates with various lattices for low-frequency vibration attenuation. J Sound Vib 2022;536:117140.
[84] Lanzoni L, Tarantino AM. Equilibrium configurations and stability of a damaged body under uniaxial tractions. Zeitschrift für Angew Math Und Phys 2015;66(1):171–90.